THE UNIVERSITY OF ALBERTA

PRECISION WAVELENGTH MEASUREMENTS OF THE VACUUM SPECTRA OF MERCURY 198 AND KRYPTON 86 IN THE VISIBLE AND ULTRAVIOLET

by

FREDERICK M. PHELPS III

A THESIS

SUBMITTED TO THE FACULTY OF GRADUATE STUDIES

IN PARTIAL FULFILMENT OF THE REQUIREMENTS FOR THE DEGREE

OF DOCTOR OF PHILOSOPHY

DEPARTMENT OF PHYSICS

EDMONTON, ALBERTA

SEPTEMBER 1963

Abstract

A Fabry-Perot Interferometer crossed with an Ebert Plane Grating Spectrograph was used to measure 26 vacuum wavelengths of Mercury 198 and 95 vacuum wavelengths of Krypton 86 in the visible and ultraviolet. The accuracies obtained are of the order of $\pm$ 0.00010 Å. From the data the corresponding wavenumbers and energy level diagrams were obtained.

Acknowledgements

The author is greatly indebted to Professor K. B. Newbound who suggested the topics investigated in this thesis and who chaired the doctoral committee. Without his valuable and frequent help and patient encouragement the project could not have been completed.

Thanks are due to the Instrument Makers, N. Riebeek, G. Sander, and J. Cuthiell who produced several essential pieces of apparatus. Their high standards of workmanship contributed significantly to the success of this work. J. Legge gave valuable help in all phases of the glass blowing required and F. Gleave gave aid with loans of apparatus from the undergraduate laboratories.

Useful ideas were obtained in discussions with many professors, graduate students, and staff members. While the list is too numerous to enumerate, special mention must be made of R. M. Ellis, P. J. Crouse, and N. Riebeek.

J. Seale, J. Seen, B. Harris, and R. Gerritsen gave considerable help with the measurements of many of the fringe diameters.

Financial support and the loan of a Krypton 86 lamp from the National Research Council of Canada are gratefully acknowledged.

Preface

Roman numerals refer to entries in the bibliography. All special symbols are defined as they are introduced and in all cases follow the recommendations of the Commission for Symbols, Units and Nomenclature of the International Union of Pure and Applied Physics.

Table of Contents

List of Tables

List of Figures

Introduction

In 1889 the Governing Committee of the International Bureau of Weights and Measures adopted as the International Meter Bar a line standard which replaced the end standard known as "Le Metre des Archives" which had served since 1799. In 1895 Michelson and Benoit measured the International Meter Bar in terms of the 6438 Å (red) line of Cadmium. The result, an accurate value in air for this wavelength, was 6438.4722 Å. An assumed correction for the water vapor pressure present in the air during their experiment* changes the value to 6438.4791 Å. In 1905 Benoit, Fabry, and Perot remeasured the bar obtaining for "Standard Air" a wavelength of 6438.4796 Å. This wavelength was adopted by Astronomers and Spectroscopists and all fundamental measurements were referred directly to it.

For practical work, or where extreme accuracy is not required, secondary standards have been adopted throughout the spectrum. These are lines whose wavelengths have been measured carefully with respect to the Cadmium red line by at least three independent investigators. Between 1889 and 1960 it became possible to measure wavelengths from isotopic sources more accurately than one could set a microscope on a line standard. Thus, at the Eleventh General Conference of Weights and Measures held in October 1960, the International Meter Bar was redefined to be exactly 1 650 763.73 wavelengths in vacuum of the 6057 Å (orange) line of Krypton 86 in an Englehard-type lamp operated at the triple point of Nitrogen.

* Hart and Baird (I) p. 782.

Several topics immediately presented themselves for study. The one selected for this thesis was to measure as many vacuum wavelengths as possible with respect to the Krypton Standard Line in the spectrum of Krypton itself and also in the spectrum of Mercury 198 in a Meggers-type electrodeless lamp. The Meggers-type lamp is useful because of its ease of excitation and high intensity. These lines are expected to serve ultimately as new secondary standards and will be approximately two orders of magnitude more accurate than current Iron and Neon secondary standards.

CHAPTER I. THEORY

1.0 Derivations of the Fundamental Equations

An interferometer of the Fabry-Perot type, called an etalon by the inventors, was crossed with an Ebert plane grating spectograph. When light from a suitable source is passed through the system the etalon forms a set of concentric circular interference fringes at infinity for each wavelength in the incident beam. These interference patterns are focused by an achromat on the entrance slit of the spectrograph. The spectrograph then disperses the interference patterns by wavelength. The result is a series of spectral emission lines with an interference pattern superimposed on each. By photographing the result, accurate relative measurements of the fringe diameters may be obtained. Using these data, precise values for the emitted wavelengths can be calculated.

The grating used in this work has 3000 lines per centimeter and was supplied by the Jarrell-Ash Company of Newtonville, Massachusetts, U. S. A.

The etalon consists of a pair of optically flat quartz plates separated by an invar spacer and held accurately parallel by springs and pressure rods.

The phase difference $\Delta\alpha$ between two points in a plane wave is*

$$\Delta\alpha = \frac{2\pi}{\lambda} \text{ (optical path difference)} \qquad (1)$$

* Jenkins and White (II) p. 184.

Consider* Figure 1. The path difference between rays 1 and 2 is AB + BC - AF. The wavelengths are different in air and in quartz since the indices of refraction of the two media are different. Writing λ_a and λ_q for the two wavelengths, the phase difference becomes

$$\Delta\alpha = \frac{2\pi}{\lambda_a}(AB + BC) - \frac{2\pi}{\lambda_q}(AF) \tag{2}$$

From Figure 1 it is clear that

$$\begin{aligned} AB &= BC = t/\cos\phi \\ AF &= AC \sin\psi \\ AC &= 2t \tan\phi \\ n_q &= \lambda_a/\lambda_q = \sin\psi/\sin\phi \end{aligned} \tag{3}$$

where n_q is the index of refraction of quartz with respect to air and Snell's law has been employed. Substituting (3) into (2) and reducing to lowest terms gives

$$\frac{\Delta\alpha}{2\pi} = P = \frac{2t}{\lambda_a}\cos\phi \tag{4}$$

where P is called the order number of the interference pattern.

Constructive interference will occur only when P is an integer. This condition is fulfilled only for certain discrete values of ϕ, namely the set ϕ_i, i = 0, 1, 2, 3, . . . Due to symmetry about the normal the interference patterns are

* This treatment of the theory is based upon Meissner (III), except for the least squares procedure.

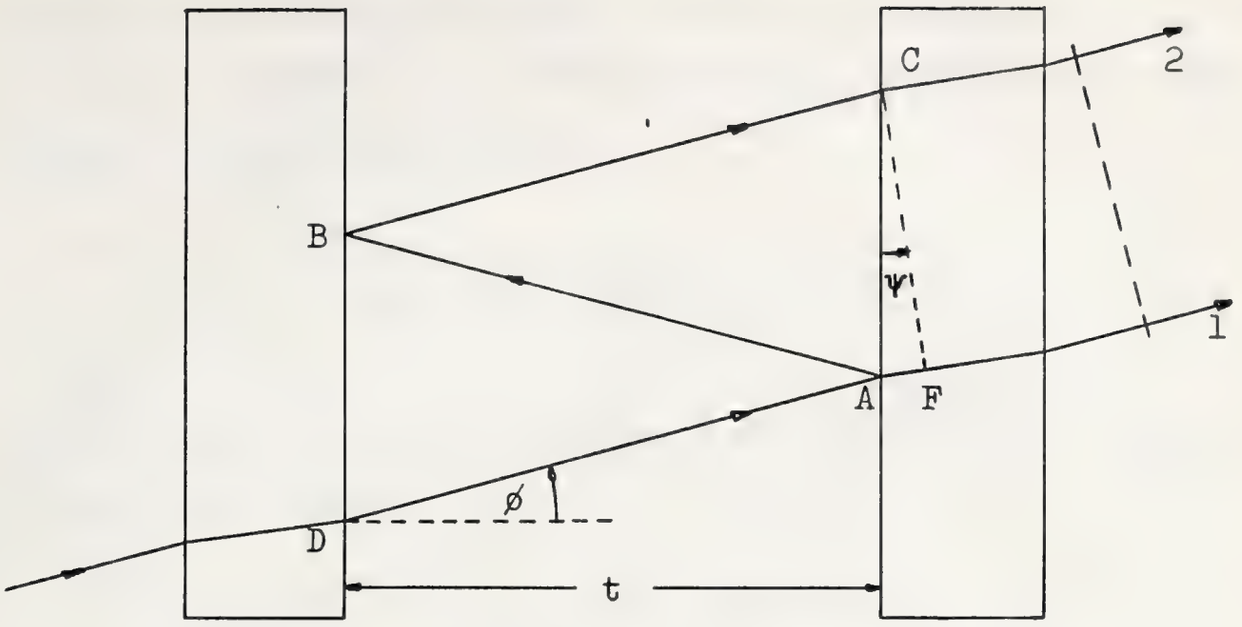

Figure 1. Schematic diagram of a Fabry-Perot etalon.

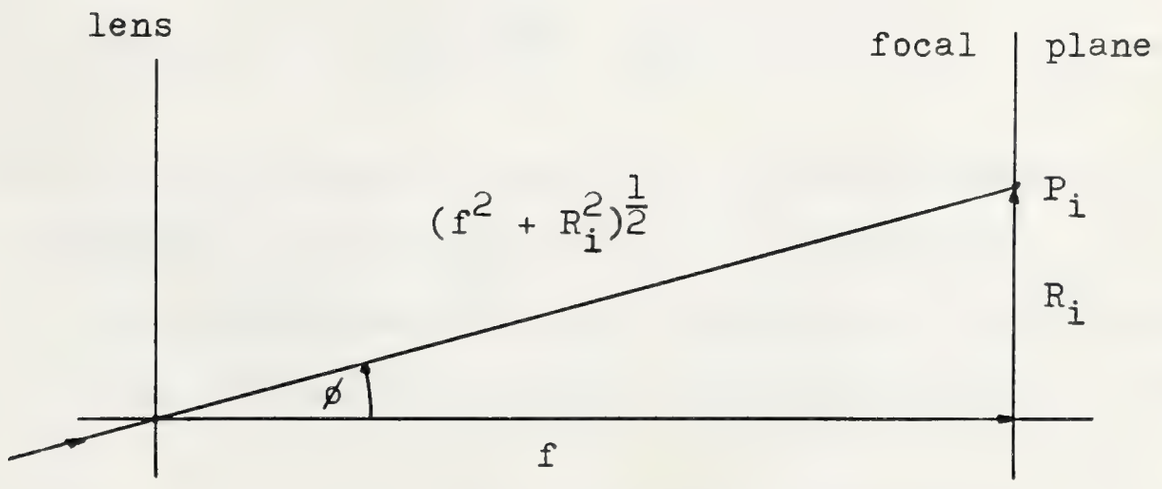

Figure 2. Formation of circular interference fringes in the focal plane of a lens.

circular in shape with their radii, R_i, depending on ϕ_i and the focal length, f, of the projecting system used. From Figure 2 one can see that

$$\cos \phi_i = f(f^2 + R_i^2)^{-\frac{1}{2}} \tag{5}$$

Expanding in a binomial series and retaining only terms to the first order gives

$$\cos \phi_i = 1 - \frac{D_i^2}{8f^2} \tag{6}$$

where $D_i = 2R_i$ is the diameter of the i^{th} ring. Substituting (6) into (4) and suppressing the subscript on λ gives

$$P = \frac{2t}{\lambda}\left(1 - \frac{D_i^2}{8f^2}\right) \tag{7}$$

This is the fundamental relation for the evaluation of the interference patterns with respect to wavelength.

Differentiating (4) with respect to ϕ and (7) with respect to D and temporarily suppressing the subscript on D yields

$$dP = -\frac{2t}{\lambda} \sin \phi \, d\phi = -\frac{2t}{\lambda}\left(\frac{2D \, dD}{8f^2}\right) \tag{8}$$

Since P has a negative slope, the order number decreases with increasing diameter or increasing angle of incidence. For $dP = -1$ we have $dD \rightarrow \Delta D$ and from (8) we find

$$-1 = \Delta D \frac{tD}{2\lambda f^2} \quad \text{or} \quad \Delta D = -\frac{2\lambda f^2}{tD} \tag{9}$$

so that ΔD decreases as D increases. This means that the rings become closer together as we proceed outward from the center of the interference pattern. Furthermore, with f and t fixed, the rings of shorter wavelength are closer together than the rings of longer wavelength. To the first order, P is a quadratic function of D so that to equal increments of P there correspond equal increments of D^2. Choosing the diameter of the innermost ring to be D_o, the following diameter D_1 and so on, D_k will be the diameter of the (k + 1) ring. We now assign to the order number P in (7) the same subscript that we assign to the diameter. The difference in order numbers between the i^{th} and k^{th} circles, $i < k$, is $P_i - P_k$, a small integer equal to k-i since $P_k < P_i$ and P_i decreases for increasing D_i. Hence

$$P_i - P_k = k - i = (D_k^2 - D_i^2) \frac{t}{4\lambda f^2} \tag{10}$$

And since from (9)

$$2D\Delta D = \Delta (D^2) = \frac{4\lambda f^2}{t} , \tag{11}$$

(10) becomes

$$\frac{D_k^2 - D_i^2}{k - i} = \Delta (D^2) \tag{12}$$

The sequence D_o^2, D_1^2, D_2^2, . . . is an arithmetic progression

with common difference $\Delta(D^2)$.

We assign an integral order number to each bright fringe. More precisely since the intensity distribution in the fringes is known to be approximately parabolic near the maximum (see Appendix II), we should assign this integral order number to the maximum intensity of each bright fringe. Any point on the interference pattern between two bright fringes will not have an integral order number, but we may assign to it a fractional order number ϵ which varies continuously from one bright fringe to the next. To the center of the interference pattern, $\phi = 0$, we assign a nonintegral order number P which we write as $P = P_0 + \epsilon = P_i + i + \epsilon$. Solving for P_i, substituting into (7), rearranging terms and making use of (11) and (12) gives

$$\epsilon = \frac{tD_i^2}{4\lambda f^2} - i = \frac{D_i^2}{\Delta(D^2)} - i \qquad (13)$$

If only the two innermost circles are available for measurement we have immediately $\Delta(D^2) = D_1^2 - D_0^2$. And (13) becomes $\epsilon = D_0^2/(D_1^2 - D_0^2)$. In high precision work many diameters are available for measurement. If an accurate value for $\Delta(D^2)$ can be found then we may write for $j = 1, 2, \ldots$ ${}^jD_0^2 = D_j^2 - j\Delta(D^2)$. Each value of D_0^2 calculated from this equation is different so they have been labeled with a presuperscript. The best value for D_0^2 is then the average $\langle D_0^2 \rangle = \sum_{j=0}^{k} {}^jD_0^2/(k+1)$. A simple scheme employing the method of least squares can be set up to obtain the average values $\langle D_0^2 \rangle$ and $\langle \Delta(D^2) \rangle$ and from them a least squares value of ϵ may be derived.

The equation $D_i^2 = \Delta(D^2)i + D_0^2$ is linear and in the standard form $y = mx + b$. The left side is now regarded as a measured value for D_i^2, while the right side is not necessarily equal to the measured left side but is regarded as being calculated from $\Delta(D^2)$ and D_0^2. We require that the sum of the squares of the deviations

$$\Sigma \left[D_i^2 - (\Delta(D^2)i + D_0^2) \right]^2$$

be a minimum. That is, we require the variations with respect to the two parameters $\Delta(D^2)$ and D_0^2 to vanish independently. This results in the following equations:

$$\Sigma i D_i^2 = \Delta(D^2)\Sigma i^2 + D_0^2 \Sigma i \tag{14}$$

$$\Sigma D_i^2 = \Delta(D^2)\Sigma i + n D_0^2 \tag{15}$$

We have used the fact that $\sum_{i=0}^{n-1} D_0^2 = nD_0^2$, where n is the number of diameters used. If D_0^2 and $\Delta(D^2)$ are eliminated from (13), (14) and (15) we find on solving for ϵ

$$\langle \epsilon \rangle = \frac{\Sigma i^2 \Sigma D_i^2 - \Sigma i^2 \Sigma i D_i^2}{n\Sigma i D_i^2 - \Sigma i \Sigma D_i^2} \tag{16}$$

$\langle \epsilon \rangle$ is taken to mean the least squares value of ϵ.

Because it is a tedious job to calculate fractional order numbers from (16) with a desk calculator, and also because arithmetical mistakes are easily made, it was desirable to program

(16) so that the calculations could all be performed by the IBM 1620 computer. Meissner is reported to have said that little improvement in the standard deviation of ϵ is obtained when more than five diameters are included in the least squares calculation. In several cases we found that up to fifteen diameters could be measured. However, least squares calculations using from six to ten diameters gave no noticeable improvement in the standard deviation of ϵ. For this reason, and also because a standard format is required for machine calculations, five diameters are always taken. Then (16) reduces to the simpler form

$$\epsilon = \frac{3\Sigma D_i^2 - \Sigma i D_i^2}{\frac{1}{2}\Sigma i D_i^2 - \Sigma D_i^2} \tag{17}$$

It is also possible to obtain from the variational calculation a least squares value for $1/\Delta(D^2)$. Multiplying (14) by n and (15) by Σi and solving the resulting equations for $1/\Delta(D^2)$ we find, on limiting ourselves to five fringes that,

$$\frac{1}{\Delta(D^2)} = \frac{5}{\frac{1}{2}\Sigma i D_i^2 - \Sigma D_i^2} \tag{18}$$

Once $1/\Delta(D^2)$ is obtained from (18) individual values of ϵ for each diameter can be calculated from (13). The average of the ϵ_i so calculated must be identical to $\langle\epsilon\rangle$. This fact serves as the only adequate check on a hand calculation of a least squares ϵ. Once the ϵ_i are obtained, the standard deviation of the mean may be calculated from the usual formula

$$\sigma = \sqrt{\frac{\sum_{i=0}^{4} (\langle \epsilon \rangle - \epsilon_i)^2}{5(4)}} \tag{19}$$

1.1 Application of the Fundamental Equations

At the center of any interference pattern, $\phi = 0$, we see from (7) that

$$(P_0 + \epsilon)\lambda = 2t \tag{20}$$

Initially, neither P_0, ϵ, λ, nor $2t$ is known. However, from (17) a value for ϵ may be calculated which is accurate to two or three significant figures. From the M.I.T. Wavelength Tables a value for λ in air may be found which is accurate to five or six significant figures. Finally an approximate value of $2t$ may be obtained by measuring the etalon spacer with a micrometer.

Consider two wavelengths, λ_a, and λ_b, found from the table. Then dropping the subscript 0 on P_0 and using (20) gives

$$\begin{aligned} (P_a + \epsilon_a)\lambda_a &= 2t_a \\ (P_b + \epsilon_b)\lambda_b &= 2t_b \end{aligned} \tag{21}$$

P_a and P_b are selected so that $2t_a$ and $2t_b$ are each smaller than the micrometer value of $2t$ by about 0.01 mm. Then P_a and P_b are increased as necessary until $2t_a = 2t_b$ to five parts in the eighth significant figure or better. One finds apparent matches in these values of $2t$ at intervals of a few tens to a few hundreds of order numbers depending on the separation of the wave-

lengths and the etalon thickness. The values of P_a, P_b, and 2t for several of these apparent matches both above and below the micrometer value are recorded. This procedure has drastically limited the possible real value of 2t to one of a small set of numbers. This limits the possible integral order number P_c which a third wavelength λ_c can have. We therefore look for values of P_c such that $2t_a = 2t_b = 2t_c$. With small spacers only a single match is expected. However with longer spacers additional wavelengths must be introduced until one unambiguous value of 2t is found. For the 10 cm. spacer used in this work nine lines were required. This procedure establishes the correct integral order numbers for each interference pattern. Threrfore we now know $(P_0 + \epsilon)$ for each pattern to an accuracy limited only by our ability to measure the relative fringe diameters.

The wavelength λ_s of the 6057 $\mathring{A}$ line of Krypton 86 is known by definition. In work of the highest precision this line must be recorded on each spectrogram so that the absolute thickness of the etalon can be found. The accuracy of $2t_s = (P_s + \epsilon_s)\lambda_s$ is limited only by our ability to measure ϵ_s and is of the order of a few parts in 10^{10}. We now use $2t_s$ and the order number for each interference pattern to calculate the wavelength of the light producing it

$$\lambda_i = \frac{2t_s}{P_i + \epsilon_i} \tag{22}$$

If the standard line does not occur on the plate several secondary standards may be used simultaneously to give an acceptable

value of 2t provided that these lines have been measured with respect to the standard, preferably in the laboratory where the work is being performed.

To apply the described method, quite accurate wavelengths are needed to establish unambiguously the integral order number. The M.I.T. wavelength tables are adequate to the task in the case of the smaller spacers with integral order numbers less than about 100,000. The more accurate interference wavelengths calculated from the thin etalons are required when the work is carried to longer etalons. Alternately, one may compare the same line from two long spacers to eliminate any uncertainty in P_0 which is usually only $\pm$ 1.

1.2 Phase Change on Reflection

When wavelengths λ_i are determined with respect to the standard line λ_s as described here, one may find a systematic variation of results with increasing etalon thickness. This is due to the fact that a phase change may occur on reflection from a metallic film. Suppose that a phase change of ray 2 with respect to ray 1 in Figure 1 is, $2\epsilon/2\pi = \delta = 2\tau/\lambda$. The last step follows from (7) when we confine ourselves to the center of the pattern. Thus the effect is a small correction τ to the geometrical length t of the etalon. The t appearing in (7) must be replaced by $t + \tau$. The order numbers n_s', and n_s'' at the center of the patterns for the standard line at two etalon thicknesses t_1 and t_2 are

$$n_s' = \frac{2t_1}{\lambda_s} + \frac{2\tau_s}{\lambda_s}$$

$$n_s'' = \frac{2t_2}{\lambda_s} + \frac{2\tau_s}{\lambda_s}$$

with similar equations for the unknown line λ_i

$$n_i' = \frac{2t_1}{\lambda_i} + \frac{2\tau_i}{\lambda_i}$$

$$n_i'' = \frac{2t_2}{\lambda_i} + \frac{2\tau_i}{\lambda_i}$$

If there is no dispersion of this phase change then $\tau_s = \tau_i$ and no error is introduced by neglecting the entire correction. In general, however, $\tau_s \neq \tau_i$ and the correction must be included in work of the highest precision. Subtracting the equations in pairs to eliminate the phase shifts, dividing the results and solving for λ_i gives

$$\lambda_i = \lambda_s \left(\frac{n_s'' - n_s'}{n_i'' - n_i'}\right) \qquad (23)$$

Other methods of making this correction are discussed in Meissner (III) pp 423 - 426.

No systematic phase change could be detected using all of the data from all of the spacers. However, there did appear to be some random fluctuations. Thus, no phase change correction could be included, though a small one may be present.

CHAPTER II. APPARATUS

2.0 The Optical Flats

The quartz optical flats used in this work have a diameter of 60 mm and a thickness of 15 mm. The second surface makes an angle of about 15' of arc with respect to the optically flat surface so that reflections from the second surfaces are not passed into the spectrograph.

The pair of flats used for all work reported here was obtained many years ago from Hilger and Watts Limited. The accuracy of the figure is not known, but since the flats must be about 40 years old, it is doubtful that they are better than 1/20 wavelength.

A new pair of flats was purchased from Englehard Industries with the same dimensions as the old flats and which were presumably accurate to 1/200 wavelength. Several pairs of photographic plates were exposed with the new flats and in all cases the results were very poor. A few lines measured with these new flats are included in the mercury data where the interference patterns were as sharp as with the old flats. However, it was found necessary to employ the Hilger and Watts flats to obtain consistent data.

2.1 Partially Reflecting Metallic Films

If the flat surfaces of the etalon are uncoated about 4% of the incident beam will be reflected at each surface and the rest will be transmitted if we neglect absorption. This means

That the intensity ratio of rays 1 and 2 in Figure 1 will be about 1600 to 1. It is impossible to believe that measurable interference patterns will form under these conditions. If a thin metal film is deposited on the flats the intensity ratio will drop but more importantly a large number of rays produced by multiple reflection will contribute to the interference pattern. Meissner (III) p 411, has shown that the instrument half width decreases rapidly with increasing reflectivity or film thickness. This means that the interference patterns become much sharper. However, this also increases the exposure time. A suitable compromise lies between 85% to 95% reflectivity. The plates used in this work had about 92% reflectivity. Aluminum films were chosen because of ease of evaporation, stability with age, absence of absorption bands and absence of serious dispersion in the reflectivity in the visible and ultraviolet. The details of the aluminization process carried out in this laboratory are given in Appendix I.

2.2 Manufacture of the Etalon Spacers

A solid bar of free machining annealed Invar was obtained 6.35 cm in diameter. From this stock six spacers were made with the following dimensions:

Outside diameter	6.0 cm
Inside diameter	5.0 cm
Nominal lengths	0.5, 1, 2.5, 5, 10, 20 cm
Area of each boss	25 mm^2

Because none of these dimensions are critical, the tolerances allowed were ± 10%.

It was found that very careful workmanship in the machine shop resulted in the spacers being sufficiently accurate to give poor interference patterns without any grinding or lapping. The smallest four spacers can be tested with a sodium or thallium lamp but a mercury 198 or krypton 86 lamp must be used to test the longer spacers. New plate glass proved to be a satisfactory surface to lap against. Indeed, some of the plate glass was so flat that Haidinger interference fringes were observed in the glass!

All bosses are first ground equally with a slurry of #175 aluminum oxide in distilled water on a new area of the plate glass until all bosses acquire a uniform black appearance as seen through an optical loupe. This removes any small ridges or burrs left in the milling and machining operations. A fresh area of glass is selected and the high boss or bosses are further ground with more of the same abrasive while the low boss or bosses are used as pivots and are lubricated with a slurry of cerium oxide in distilled water. Equal lapping is done on each end of the spacer. After a few strokes, the spacer is thoroughly washed and dried and the bosses inspected. Any abrasive particles missed by the washing or lint left by the drying are brushed away. The interferometer is assembled and tested and the high bosses are recorded. The difference from the previous recording is noted. The procedure is repeated as necessary.

In this way the 0.5 cm spacer was lapped until the separations of opposite pairs of bosses differed by less than half a wavelength (one fringe) in about three days. A correction of this magnitude can be made by the springs and pressure rods of

the etalon holder. The next three spacers were lapped to the same or better tolerances in about one day each. The 10 cm spacer was lapped in very rapidly, being almost perfect after the fourth attempt. No attempt has yet been made to put the 20 cm etalon into operation. If the lapping does not proceed uniformly, either insufficient care is being exercised in the cleaning of the spacer and mirrors before assembling the etalon for a test, or the glass has become frosted. If the latter occurs, the lapping will not be predictable and the bosses will become badly rounded. The author found that if new glass is used for each step, then five strokes on each end will reliably remove 2500 Å of metal from the high boss.

2.3 The Comparator and Measurement of the Fringe Diameters

To evaluate the partial order numbers the diameters of five consecutive Fabry-Perot fringes must be measured. Traditionally the diameters were measured directly from the spectroscopic plates by eye through a travelling microscope. This procedure is open to two objections. Operator fatigue is so great that many errors are made in any long session. This wastes computing time and corrections can be made only if the plate is remeasured. A more serious objection, however, is that the eye cannot distinguish between the maximum intensity and the center of a given fringe. In practice, one always sets the microscope on the center while theory demands that one set on the maximum intensity of the fringe. These two positions are not necessarily identical, and it is believed that the limiting accuracy found in the literature,

about 0.0005 Å, is a result of this effect. We have, therefore, developed a scheme to circumvent both of these problems. It gives an improvement of one order of magnitude in accuracy.

Instead of scanning the plate by eye, an electro-optical system is used. A line filament lamp is placed at the focal point of a small achromat. Thus, light from the lamp is rendered parallel and falls on an adjustable slit. The image of the slit is focused by a microscope objective onto the spectroscopic plate to be measured. The plate rests on the bed of an old comparator which is used for its accurate ways and screw. The transmitted light is focused by a second microscope objective onto a second slit behind which is a DuMont 6291 photomultiplier tube. As the photographic plate is moved through the light beam, the photomultiplier current varies and hence a varying voltage develops across the anode resistor. This varying voltage is amplified by a two stage emitter follower amplifier to match impedances and is fed into a Bristol recording potentiometer. The pen of the recorder traces out the variations of intensity of the interference pattern giving a trace that resembles a sine wave. The chart drum is connected directly through two gears to the comparator screw so that there is a one to one correspondence between points on the chart paper and points on the plate. The expansion of the photographic image to the chart trace is 1 to 1143. A major source of error in this method is that we must rely on the chart manufacturer to punch the chart drive sprocket holes uniformly with respect to the engravings on the paper. Occasionally, jump discontinuities of the order of 0.01 inch between adjacent lines in the chart engraving

are observed. No attempt has been made to correct for either of these sources of error.

The peaks on the chart paper which correspond to the dark fringes in the interference pattern are split in several points with a steel ruler. A smooth curve through these points is drawn and extended until it intersects the trace. The intersection point is read with an optical loupe of moderate power to 0.01 inch. The values obtained are recorded in notebooks. Appropriate subtractions give the relative diameters which are then punched into IBM cards. The 1620 processes the cards in 2.3 seconds each giving the least squares partial order number, the individual partial order numbers and the standard deviation. A Marchant hand calculation takes 15 minutes.

A schematic diagram of the photomultiplier circuit and the transistor amplifier follow.

2.4 The Spectrograph

A stigmatic 3.4 meter Ebert plane grating spectrograph, supplied by the Jarrell-Ash Company of Newtonville, Massachusetts, was used in this work. Since the mounting is not yet common, a brief description follows. Light falling on the entrance slit, situated at the center of one end of a light tight box 70 cm wide, 60 cm high, and 340 cm long, is reflected from a spherical mirror of 40 cm aperture at the far end of the box to a plane grating mounted 200 cm from the mirror. The light which is reflected from the grating again strikes the mirror and is brought to a focus in a slightly curved cylindrical surface of radius 500 cm immediately

Figure 3. A schematic diagram of the photomultiplier circuit and the emitter follower amplifier built for use with the recording potentiometer.

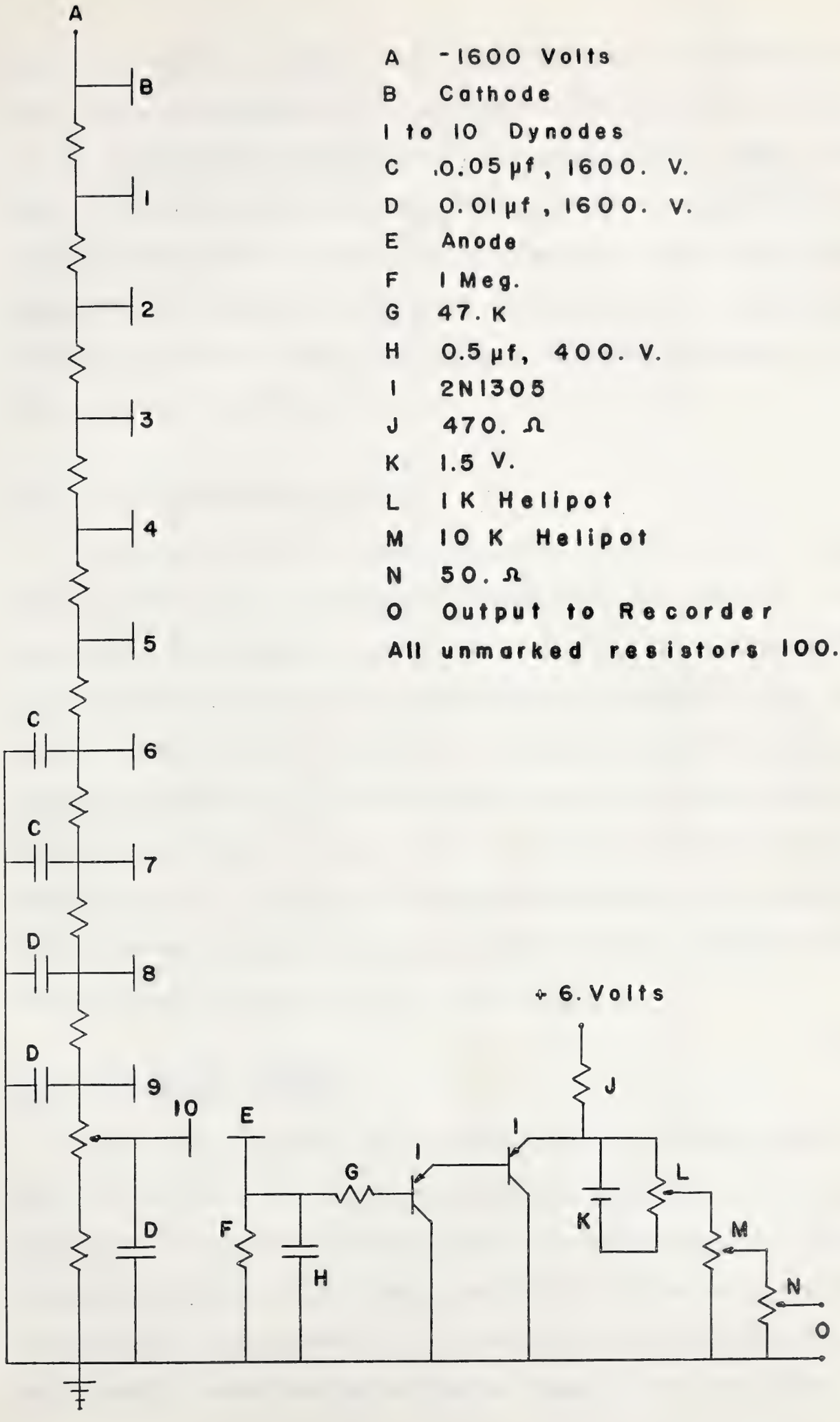

A -1600 Volts
B Cathode
1 to 10 Dynodes
C .0.05 μf, 1600. V.
D 0.01 μf, 1600. V.
E Anode
F 1 Meg.
G 47. K
H 0.5 μf, 400. V.
I 2N1305
J 470. Ω
K 1.5 V.
L 1 K Helipot
M 10 K Helipot
N 50. Ω
O Output to Recorder
All unmarked resistors 100. K.

above the entrance slit. With the 3000 line/centimeter grating used here, a dispersion of 50 Å/mm in the 2nd order, and 25 Å/mm in the 3rd order was obtained. The plate holder takes two standard 4" x 10" plates end to end and gives excellent coverage of the spectrum from the infrared through the ultraviolet with each exposure. The optical alignment and focus of the spectrograph were very carefully adjusted using a Hartmann diaphram before the experiments were begun.

2.5 The Photographic Plates

Only Kodak 103-F plates were used in this work. The spectral response is quite uniform from about 7000 Å to 2500 Å. They are moderately fine grained, and fairly fast. Kodak type 1-N plates were ordered to extend the measurements to 9000 Å, but failed to arrived. The plates were always developed immediately after exposure in D-19 for 5^m at 18^o C with continuous hand agitation. The plates were fixed in Kodak acid fixer for 15^m and washed in running water for 30^m. To aid in uniform development, the plates were dipped in water to wet the emulsion and eliminate bubbles immediately before being plunged into the developer.

2.6 The Vacuum Chamber

The vacuum chamber is an aluminum tube 76 mm inside diameter and 300 mm long. It is fitted with a removable flange at one end and sealed shut with a heavy plate at the other end. Each end has a quartz window,with a clear aperture of 18 mm,held in place by vacuum wax. The chamber is connected through a liquid air trap and a small one-stage Hg diffusion pump to the fore pump. The

chamber pressure is monitored with a McLeod Gauge. When in operation, pressures from 0.12 to 0.03 x 10^{-3} torr are obtained. Surrounding the vacuum chamber is an aluminum box containing 20 liters of water. This box is surrounded by 5 cm of vermiculite insulation and an outer shell of 3/4 inch plywood. Because of the long time constant, changes in room air temperature have no detectable effect on the etalon when exposures of 1/2 hour or less are made. Previously, however, small changes in etalon length were observed when 7 hour exposures were required. During construction, provision was made to hold the temperature of the water bath constant within $\pm$ 0.01°C near 15 °C and to measure a gas pressure in the etalon chamber of 1 atmosphere to $\pm$ 10^{-3} torr. Details of the heater, cooling coil, thermostat, and barometer are not included here since they are irrelevant to the topic under discussion. The light from the source under study was focused inside the etalon with a quartz-fluorite achromat. The Fabry-Perot fringes formed were then focused on the entrance slit of the spectrograph with a second lens of 25 cm focal length. Since it is necessary to photograph exactly the diameter of the ring system, the optical system must be aligned with care before each series of exposures.

Since the fringes are not intense enough to be seen on the entrance slit, the adjustment is accomplished as follows. The plate holder is replaced by a 100 watt incandescent lamp and the light is sent through the spectrograph in the reverse direction. The image of the slit which is reflected from the etalon is made to coincide with the slit itself by adjusting the leveling screws which support the etalon chamber, and with the traverse screws at

the rear of the box. The front leveling screw is a pivot while the rear leveling screws slide easily on a 1/2" thick aluminum plate bolted to the spectrograph's optical bar.

2.7 The Mercury Lamp and Exciters

The Meggers-type electrodeless Hg 198 lamp, a sealed quartz tube 150 mm long x 8 mm diameter containing when new 0.4 mg mercury 198, 4 torr argon, and 6 torr xenon, was purchased from Baird Atomic, Cambridge, Massachusetts. The lamp is operated by subjecting it to high frequency electromagnetic radiation. Originally, a war surplus radar set operating at a frequency of 600 megacycles was used. But because of poor coupling to the lamp, exposures as long as 6^h45^m were found necessary to bring up moderately strong mercury lines. Also, replacement triodes proved a problem for the newest ones available were made 20 years ago (1943) for the United States Navy. Finally so much trouble developed that the radar set was retired and a Raytheon Microtherm Generator operating at 2.45 gigacycle was purchased. This generator is able to supply up to 100 watts of microwave power but was never operated at a power level greater than 40 %. The generator is fitted with a matched coaxial cable and reflector so that most of the power reaches the lamp. Exposures longer than a few seconds overexpose the 2537 Å line while the faintest lines measured reach suitable photographic densities after 10 minutes. The lamp must be operated in a cooling blast of air from a small hair dryer. When this is not done, the lamp becomes so hot that the interference maxima overlap as a result of Doppler broadening.

2.8 The Standard Krypton Lamp

Based on the advice of Baird (IV) and of Hart* of N.R.C. an Englehard-type Kr 86 lamp was built which contained a quartz window. This lamp failed to ignite and was unfortunately broken during an attempt to shorten the high voltage terminal. Hart loaned us another lamp which, however, contained only a glass window so that the ultraviolet lines were inaccessible. A second lamp with a quartz window was built but is not yet operational. The Englehard-type lamp must be operated at the triple point of nitrogen. It is contained in a large Dewar fitted with a lucite top through which passes the arm fitted with a quartz or glass window, the high voltage lead and filament connections. The triple point is easily reached by pumping for a few minutes on a Dewar full (5 liters) of liquid nitrogen with a 140 ℓ/min. fore pump. The exhaust gases are passed through a glass-wool filter to remove the oil vapor picked up on passage through the pump.

2.9 The Electrodeless Krypton Lamp

An electrodeless Kr 86 lamp containing 6 torr of gas, and a microwave cavity designed for use with the Raytheon Microtherm Generator, were obtained from the Opthos Instrument Company, Rockville, Maryland. The spectrum of this lamp was investigated with the 1 cm etalon when the lamp was operated in air and when the cavity and lamp were operated submerged in boiling liquid air to a depth just sufficient to keep the lamp from being completely

*Private communication with K. H. Hart.

covered. Many lines of the krypton spectrum found with the Englehard lamp are not visible with the electrodeless one and the lines are quite broad due to pressure and temperature effects. It is, therefore, not a suitable source in its present form for high precision work.

CHAPTER III. DATA

3.0 Etalon Thicknesses

Approximate etalon thicknesses, as determined from the 6057 Å line are tabulated here for future reference. An assembled etalon is found to hold its adjustment for many months if stored in the vacuum chamber. However, it is necessary to take the etalons apart from time to time in order to change the spacer. It is never possible to reproduce the thickness exactly, but by using the same set of springs, one usually comes within 0.000 05 cm of the tabulated values.

Table I
Etalon Thicknesses

Nominal Value of t	Measured Value of 2t
0.5 cm	1.097 166 cm
1.0 cm	2.048 396 cm
2.5 cm	5.345 840 cm
5.0 cm	10.103 537 cm
10.0 cm	19.971 650 cm

3.1 Photographic Plates Measured

About 100 Kodak type 103-F 4" x 10" spectrographic plates were exposed. Of these, only certain pairs were measured. Whenever a pair of plates was measured at all, every possible interference pattern on the plate was measured. Each pattern due to the 6057 Å line was always measured three times and the mercury secondary standards on the plates which did not contain the

krypton spectrum were measured two or three times. Six exposures were made on each photographic plate. The slit length was 14 or 10 mm, and its width the maximum obtainable, about 1/2 mm. The grating was set at 4.80° since the optimum range of wavelengths and intensity was found here.

The exposure sequence on each pair of plates wes a basic time t, determined from a test exposure plate, followed by additional exposures of 3t, 6t, 9t, 6t, 3t, except on a few plates where the sequence was t, 3t, 6t, 6t, 3t, t. The range of t was from 1 minute with the Kr 86 Englehard lamp to 15 minutes for the Hg 198 lamp operated with the radar set. This means the longest exposures were from 27 minutes to 6 hours 45 minutes.

Nearly 600 spectra were photographed for this thesis and about 4500 least square calculations were made on 2757 interference patterns.

3.2 The Spectrum of Mercury 198

All of the mercury data obtained from six pairs of 5 cm plates and two pairs of 10 cm plates is averaged and presented in Table III. The first column is an ordinal number assigned to each line and will be useful later. The second column gives the number of interference patterns measured and averaged into the final result. The third column contains the wavelength and the fourth column the standard deviation. The errors in the ϵ's calculated from (19) appear to have little to do with the accuracy involved. Using them, the standard deviation of the mean is about $\pm$ 0.00001 Å for all lines for which 20 or more interference

Table II

Plates Measured

Plate Number	Etalon Spacing	Light Source(s)
11	0.5 cm.	Hg 198
12	0.5 cm.	Hg 198
13	0.5 cm.	Hg 198
26	1.0 cm.	Hg 198 and Kr 86 Electrodeless
27	1.0 cm.	Kr 86 electrodeless in liquid air
31	1.0 cm.	Hg 198 in liquid air
17	2.5 cm.	Hg 198
18	2.5 cm.	Hg 198
19	2.5 cm.	Hg 198
14	5.0 cm.	Hg 198
15	5.0 cm.	Hg 198
16	5.0 cm.	Hg 198
23	5.0 cm.	Hg 198 New flats
24	5.0 cm.	Hg 198 New flats
38	5.0 cm.	Hg 198 and Standard Kr
33	10.0 cm.	Hg 198
35	10.0 cm.	Hg 198 and Standard Kr
36	10.0 cm.	Hg 198 and Standard Kr

patterns are available. This is ridiculously small since the variation from one plate to another is 10 to 20 times this amount. One should not expect the mean value to be influenced strongly by a single additional observation when it is the average of 20 or more values. Thus, the only meaningful error which can be stated here is the standard deviation calculated from

$$\sigma = \sqrt{\frac{\sum_{i=1}^{n} (\bar{\lambda} - \lambda_i)^2}{n}} \qquad (24)$$

All measurements were given equal weight for no objective criterion could be found to weight them differently. Several calculations were made in which the measurements were weighted with the inverse square of the standard deviation calculated from (19) as recommended by Parratt (XVII) p. 118. No improvement over a simple mean was evident and indeed there was some indication that such a procedure led to poorer results. In work of the precision sought here, one must always be on guard against excessive optimism. It is far better to give estimates of the errors ten times too large than ten times too small.

The wavenumbers in kaysers are given in column five and the two energy levels for the particular transition are given in columns six and seven for assumed Russell-Saunders coupling.

At 2.5 cm. the resonance line at 2537 Å was measured. No pattern was visible at greater etalon separations due to its large line width. A dividend was also obtained in that at 2.5 cm two of the strongest lines in the xenon spectrum were recorded with sufficient intensity to measure. Finally at 0.5 cm several

mercury lines not resolved with other etalon spacings were measurable. The 2.5 and 0.5 cm data are recorded in Table IV using the same format as Table III. The large errors in Table IV are an indication of the fact that the integral order number is not large enough to mask the error in the fractional order number.

The Meggers-type Hg 198 lamp employed in this work was filled initially with 0.4 mg Hg 198, 4 torr argon, and 6 torr xenon. Thus fairly large pressure shifts for most lines of the spectrum must be expected. Unfortunately one can neither control nor measure the pressure in this type of lamp so that only an educated guess can be given as to its effect on the spectrum. The author is aware of only three papers, Kaufmann (XXVIII), Jackson (XVIII) and Baird and Smith (XX), in which experimental determinations of pressure corrections have been reported. There is no satisfactory theory by which the shifts can be calculated. Baird and Smith (XX) showed that the 5462 Å line is shifted to the red by 0.00006 Å per torr argon pressure. Assuming that xenon will have about the same effect as argon since they are both inert gases, we expect a shift in this lamp for this line of 0.0006 Å. Since the accepted value for this line is 5462.2705 Å we expect to find 5462.2711 Å. The measured value from 37 interference patterns obtained with the 5 and 10 cm spacers simultaneously with the standard line gives, 5462.27113 Å $\pm$ 0.00027 Å, very good agreement indeed.

On the other hand Kaufman's data predicts a much larger pressure shift of 0.00010 Å per torr argon pressure. However, his zero pressure wavelength is 5462.27036 Å, indicating that we

Table III 5 and 10 cm Hg 198 Wavelengths.

#	Mean of	λ and σ in 10^{-14}m	$\bar{\nu}$ in cm^{-1}	Low term	High term
1	2	5891 9281.6 ± 1.8	16 972.3726	$6s7s\,^1S_0$	$6s10p\,^3P^o_0$
2	20	5792 2689.5 ± 0.8*	17 264.3917	$6s6p\,^1P^o_1$	$6s6d\,^1D_2$
3	21	5771 1994.0 ± 3.0	17 327.4207	$6s6p\,^1P^o_1$	$6s6d\,^3D_2$
4	37	5462 2711.3 ± 2.7	18 307.4032	$6s6p\,^3P^o_2$	$6s7s\,^3S_1$
5	23	4359 5625.2 ± 1.1	22 938.0814	$6s6p\,^3P^o_1$	$6s7s\,^3S_1$
6	34	4078 9895.2 ± 0.2	24 515.8757	$6s6p\,^3P^o_1$	$6s7s\,^1S_0$
7	35	4047 7147.9 ± 0.6	24 705.2980	$6s6p\,^3P^o_0$	$6s7s\,^3S_1$
8	62	3664 3244.5 ± 0.7	27 290.1598	$6s6p\,^3P^o_2$	$6s6d\,^1D_2$
9	65	3655 8806.7 ± 0.7	27 353.1904	$6s6p\,^3P^o_2$	$6s6d\,^3D_2$
10	70	3651 1968.3 ± 0.2	27 388.2797	$6s6p\,^3P^o_2$	$6s6d\,^3D_3$
11	14	3342 4424.3 ± 2.3	29 918.2416	$6s6p\,^3P^o_2$	$6s8s\,^3S_1$
12	33	3132 7500.0 ± 1.5*	31 920.8363	$6s6p\,^3P^o_1$	$6s6d\,^1D_2$
13	39	3126 5761.6 ± 1.2	31 983.8682	$6s6p\,^3P^o_1$	$6s6d\,^3D_2$
14	2	3024 3572.6 ± 2.1	33 064.8767	$6s6p\,^3P^o_2$	$6s7d\,^3D_2$
15	10	3022 3797.6 ± 1.7	33 086.5106	$6s6p\,^3P^o_2$	$6s7d\,^3D_3$
16	24	2968 1498.5 ± 1.4	33 691.0214	$6s6p\,^3P^o_0$	$6s6d\,^3D_1$
17	5	2894 4465.4 ± 4.2	34 548.9193	$6s6p\,^3P^o_1$	$6s8s\,^3S_1$

* Double line, not resolved.

Table IV 2.5 and 0.5 cm Hg 198 Wavelengths

#	Mean of		λ and σ in 10^{-14}m	$\bar{\nu}$ in cm^{-1}	Low term	High term
			2.5 cm data			
1	30		2537 2683.9 ± 0.2	39 412.4644	$6s6s\,^1S_0$	$6s6p\,^3P_1^o$
2	4	Xe	4672 5338.8 ± 3.8	21 401.6640		
3	2	Xe	4625 5714.4 ± 2.5	21 618.9505		
			0.5 cm data			
4	3		4348 7181.5 ± 5.5	22 995.2820	$6s6p\,^1P_1^o$	$6s7d\,^1D_2$
5	12		3132 7475.0 ± 14.1	31 920.8618	$6s6p\,^3P_1^o$	$6s6d\,^1D_2$
6	12		3132 4572.6 ± 12.3	31 923.8194	$6s6p\,^3P_1^o$	$6s6d\,^3D_1$
7	2		2926 2697.4 ± 1.2	34 173.1996	$6s6p\,^3P_0^o$	$6s9s\,^3S_1$
8	4		2753 5955.7 ± 10.6	36 361.1537	$6s6p\,^3P_0^o$	$6s8s\,^3S_1$
9	4		2655 9203.0 ± 14.9	37 651.7322	$6s6p\,^3P_1^o$	$6s7d\,^1D_2$
10	4		2654 4724.0 ± 6.9	37 672.2696	$6s6p\,^3P_1^o$	$6s7d\,^3D_1$
11	10		2652 8309.7 ± 6.0	37 695.5792	$6s6p\,^3P_1^o$	$6s7d\,^3D_2$
12	1	Xe	4735 4778.1	21 117.1932		
13	1	Xe	4502 2391.4	22 211.1702		

should expect a wavelength of 5462.27136 Å. This is higher than our value and indicates that xenon may not have the same effect as argon.

Probably two of the measured lines, those at 3664 Å and 3655 Å are only slightly affected by the carrier gas pressure. These two lines involve transitions in which the total angular momentum J is invariant. One might expect that the 4359 Å line and the 4047 Å line would be affected about as much as the 5462 Å line since they all have the same higher term, namely $7s^3S_1$. This does not seem to be the case as indicated by the following experiment which was accidentally performed. The Hg 198 lamp was operated in liquid air and the usual measurements were made on one pair of plates. Using the 4359 Å line and the 4047 Å line as standards, the 5462 Å line was found to have the wavelength 5462.27056 $\pm$ 0.00043 Å. The result is not precise since only three values contribute to the average. However, one expects that the gas pressure will be considerably lower due to the low temperature. Thus the red shift due to pressure effects should be reduced, as we observe. Unfortunately this cannot be quantative since we have no way of measuring the temperature inside the lamp or of comparing it with the external temperature.

3.3 Interpretation of the Hg 198 Spectrum and Russell-Saunders Coupling

Mercury has the electronic configuration in the ground state

$1s^2 2s^2 2p^6 3s^2 3p^6 3d^{10} 4s^2 4p^6 4d^{10} 4f^{14} 5s^2 5p^6 5d^{10} 6s^2$, $^1S_0$. Thus there are two optical electrons outside a closed shell which is considered to be spherically symmetric. It is possible in principle to write down Schrödinger's Equation for this atom assuming only electrostatic interactions. The equation is not separable in the coordinates of the electrons, though suitable approximations to the potential energy function make machine calculations possible. For a full treatment, the long articles by E.U. Condon, J.R. McNalley, L. Aller, and N.F. Ramsey in the McGraw-Hill Handbook of Physics (XXI) should be consulted.

The result of such calculations can be interpreted satisfactorily with the vector model of the atom as is done in White (XXII) or Semat (XXIII) or in numerous other books on atomic structure. The optical electrons are assumed to have orbital angular momenta ℓ_i, and spin angular momenta s_i, with the units of each being $h/2\pi$. The total angular momentum and spin of the core of the atom is taken to be zero. Thus the total orbital angular momentum $\vec{L}$ is the vector sum of the individual orbital angular momenta of the two optical electrons only.

$$\vec{L} = \vec{\ell}_1 + \vec{\ell}_2$$

and similarly the total spin $\vec{S}$ is

$$\vec{S} = \vec{s}_1 + \vec{s}_2$$

The total angular momentum of the atom $\vec{J}$ is the vector sum

$$\vec{J} = \vec{L} + \vec{S}$$

Since $s = \pm \frac{1}{2}$, one finds that S = 0 or 1 only. Thus if L = 0, then J = 0 or 1; if L = 1, J = 0 or 1 or 2; if L = 2, then J = 1, 2, or 3; etc. Thus one finds two series of spectral lines, singlets in which S = 0, and triplets in which S = 1. The notation used is

$$(2S + 1)L_J$$

Allowed transitions are governed by the selection rules $\Delta J = 0, \pm 1$ with $0 \rightarrow 0$ completely forbidden; $\Delta L = 0, \pm 1$; $\Delta S = 0$. The presuperscript gives the multiplicity of the level and also the total spin quantum number. The postsuperscript o indicates the parity when it is odd. This symbol is redundant but is demanded by some spectroscopists. This notation and its interpretation is given the name Russell-Saunders or LS coupling. It is not rigidly obeyed in mercury since violation of the selection rule, $\Delta S = 0$ may be seen in Table III in entries 1, 3, 6, 8, and 12 and in Table IV entries 1, 5, and 9. However, the notation does explain the separation of the energy levels into singlets and triplets and the interpretation in terms of angular momentum is easy to understand. There can be no doubt that the energy levels and transitions are correctly stated in Tables III and IV since they are consistent with the levels given in Landolt-Börnstein (XXIV) Volume 1, p. 91. Consider, for example the following transitions from Table III.

Table V

Consistency of the Hg 198 Wavelengths

Transition $^3P_1$-$^3P_2$	Wavenumber difference in cm^{-1}
(5) - (4)	4 630.6782
(12) - (8)	4 630.6765
(13) - (9)	4 630.6778
(17) - (11)	4 630.6778
Average	4 630.6776 ± 0.0006

While the transitions listed in Table V are not extensive, the indication is that the wavelengths are accurate to 1 part in 20,000,000. since the wavenumbers are accurate to at least 1 millikayser. A few additional transformations can be studied by combining the data of Table IV with that of Table III, but doing so adds nothing of importance. A more important point is that the krypton data show the same accuracy. A comparison of the wavelengths measured here with the recent literature shows excellent agreement if one keeps in mind the fact that the literature mercury data is for Meggers-type lamps containing only 1/4 torr argon. The comparison is presented in Table VIII for both elements.

3.4 Mercury 198 Conclusions

All recent investigators report that excellent Fabry-Perot interference fringes are found for the mercury lines at 5462 Å and at 5792 Å with a Meggers-type lamp. The author did not find this to be so. The 5462 Å line in particular was found to give poorly defined fringes which were hard to measure accurately.

Indeed the variations in the patterns were so great that the only conceivable cause must be inherent in the lamp itself or in our method of exciting it. The latter is unlikely, as we used a standard radio frequency oscillator and always operated the lamp at minimum power output, usually 20 or 30 watts. We cannot understand why this line is recommended as a secondary standard, see reference (X).

It is difficult to understand why the 5792 Å line has been recommended as a secondary standard. In the case of natural mercury, this line is the well-known yellow doublet whose air wavelengths and transitions are

5790.65 Å	$6s6p\,^1P_1 - 6s6d\,^1D_2$	17 262.2 cm^{-1}
5789.66 Å	$6s6p\,^1P_1 - 6s6d\,^3D_1$	17 265.2 cm^{-1}

Surely this is not an isotopic effect so that neither line can be considered pure in a Meggers-type lamp even though the two lines were not resolved on any of our plates. The observed line at this wavelength always looked sharp, but why should the inter-combination line be totally absent in this type of discharge when it is so prominent otherwise?

The most consistent lines found in this work were those at 4359 Å, 4047 Å and at 3651 Å. If mercury 198 secondary standards are desired these should have first choice.

3.5 The Spectrum of Krypton 86

An Englehard-type krypton 86 lamp with a quartz window was designed and built and sent to the National Research Council for filling. The lamp was to be viewed along the capillary with the

anode toward the observer, as recommended by K. H. Hart in a private communication. This design was chosen so that the ultraviolet portion of the spectrum could be studied. Any other version of the lamp would have required a quartz Dewar which would have cost about $2,000. This lamp was broken before it was ever operated. The lamp which was used was borrowed from K. H. Hart of the National Research Council. While it is not strictly a standard Englehard type lamp, since its capillary is 6 mm in diameter rather than 3, it was intensively studied by Baird and Smith (IV) and is known to be as good a standard for the orange line as any other lamp if the current is maintained from 100 to 150 milliamperes. The lamp was always operated with a current of 110 ma with the anode to cathode potential adjusted to whatever value gave this current as read by a series AVO meter.

Whenever an exposure was being made, the lamp was well surrounded by a slush of nitrogen at the triple point. If the slush began to get thin, the pumping speed could be easily increased by means of a Jamesbury ball valve in the vacuum line.

Ninety-five krypton 86 lines were observed and are recorded in Table VI. One of the strongest lines in the krypton II spectrum was observed on plate 38. The average wavelength from two patterns was 4676.07650 $\pm$ 0.00016 Å. However, since it was impossible to establish unambiguously the correct integral order number, twice the etalon thickness 2t = 10.103 573 841 cm is given here so that the wavelength can be corrected by the free spectral range if necessary at some future date.

The krypton lines were much sharper than the mercury lines.

Table VI. 5 and 10 cm Wavelengths of Kr 86

#	Mean of	λ and σ in 10^{-14}m	$\bar{\nu}$ in cm^{-1}	Paschen	Lower term	Higher term
1	22	6906 5827.6 ± 1.7	14 478.9403	$2p_{10}$-$3s_5$	$(^2P^o_{1\frac{1}{2}})5p[0\frac{1}{2}]_1$	$(^2P^o_{1\frac{1}{2}})7s[1\frac{1}{2}]^o_2$
2	13	6871 5247.1 ± 0.5	14 552.8109	$2p_6$-$5d_5$	$(^2P^o_{1\frac{1}{2}})5p[1\frac{1}{2}]_2$	$(^2P^o_{1\frac{1}{2}})6d[0\frac{1}{2}]^o_1$
3	12	6848 2895.2 ± 2.8	14 602.1864	$2p_{10}$-$3s_4$	$(^2P^o_{1\frac{1}{2}})5p[0\frac{1}{2}]_1$	$(^2P^o_{1\frac{1}{2}})7s[1\frac{1}{2}]^o_1$
4	2	6830 9716.7 ± 1.5	14 639.2058	$2p_7$-$5d_6$	$(^2P^o_{1\frac{1}{2}})5p[1\frac{1}{2}]_1$	$(^2P^o_{1\frac{1}{2}})6d[0\frac{1}{2}]^o_0$
5	22	6814 9877.9 ± 0.6	14 673.5406	$2p_6$-$5d_3$	$(^2P^o_{1\frac{1}{2}})5p[1\frac{1}{2}]_2$	$(^2P^o_{1\frac{1}{2}})6d[1\frac{1}{2}]^o_2$
6	14	6741 9574.2 ± 1.9	14 832.4876	$2p_7$-$5d_3$	$(^2P^o_{1\frac{1}{2}})5p[1\frac{1}{2}]_1$	$(^2P^o_{1\frac{1}{2}})6d[1\frac{1}{2}]^o_2$
7	23	6701 0780.5 ± 0.3	14 922.9720	$2p_6$-$5d'_1$	$(^2P^o_{1\frac{1}{2}})5p[1\frac{1}{2}]_2$	$(^2P^o_{1\frac{1}{2}})6d[2\frac{1}{2}]^o_3$
8	24	6655 0704.4 ± 0.4	15 028.3952	$2p_7$-$5d''_1$	$(^2P^o_{1\frac{1}{2}})5p[1\frac{1}{2}]_1$	$(^2P^o_{1\frac{1}{2}})6d[2\frac{1}{2}]^o_2$
9	20	6578 2357.5 ± 3.0	15 201.6443	$2p_6$-$4s_5$	$(^2P^o_{1\frac{1}{2}})5p[1\frac{1}{2}]_2$	$(^2P^o_{1\frac{1}{2}})8s[1\frac{1}{2}]^o_2$
10	11	6557 5047.5 ± 4.7	15 249.7030	$2p_6$-$4s_4$	$(^2P^o_{1\frac{1}{2}})5p[1\frac{1}{2}]_2$	$(^2P^o_{1\frac{1}{2}})8s[1\frac{1}{2}]^o_1$
11	11	6538 3563.0 ± 3.2	15 294.3638	$2p_7$-$5d_2$	$(^2P^o_{1\frac{1}{2}})5p[1\frac{1}{2}]_1$	$(^2P^o_{1\frac{1}{2}})6d[1\frac{1}{2}]^o_1$
12	12	6506 7002.6 ± 1.5	15 368.7731	$2p_8$-$5d_5$	$(^2P^o_{1\frac{1}{2}})5p[2\frac{1}{2}]_2$	$(^2P^o_{1\frac{1}{2}})6d[0\frac{1}{2}]^o_1$
13	15	6489 8609.5 ± 0.4	15 408.6506	$2p_7$-$4s_4$	$(^2P^o_{1\frac{1}{2}})5p[1\frac{1}{2}]_1$	$(^2P^o_{1\frac{1}{2}})8s[1\frac{1}{2}]^o_1$

14	35	6458 0718.4 ± 1.2	15 484.4979	$2p_9$-$5d'_4$	$(^2P^o_{1\frac{1}{2}})5p[2\frac{1}{2}]_3$	$(^2P^o_{1\frac{1}{2}})6d[3\frac{1}{2}]^o_4$
15	11	6450 5803.0 ± 2.2	15 502.4812	$2p_9$-$5d_3$	$(^2P^o_{1\frac{1}{2}})5p[2\frac{1}{2}]_3$	$(^2P^o_{1\frac{1}{2}})6d[1\frac{1}{2}]^o_2$
16	39	6422 8005.7 ± 0.7	15 569.5326	$2p_8$-$5d_4$	$(^2P^o_{1\frac{1}{2}})5p[2\frac{1}{2}]_2$	$(^2P^o_{1\frac{1}{2}})6d[3\frac{1}{2}]^o_3$
17	20	6417 4515.0 ± 0.9	15 582.5097	$2p_9$-$5d_4$	$(^2P^o_{1\frac{1}{2}})5p[2\frac{1}{2}]_3$	$(^2P^o_{1\frac{1}{2}})6d[3\frac{1}{2}]^o_3$
18	20	6375 3511.6 ± 1.1	15 685.4105	$2p_8$-$5d''_1$	$(^2P^o_{1\frac{1}{2}})5p[2\frac{1}{2}]_2$	$(^2P^o_{1\frac{1}{2}})6d[2\frac{1}{2}]^o_2$
19	4	6353 6699.4 ± 5.8	15 738.9353	$2p_8$-$5d'_1$	$(^2P^o_{1\frac{1}{2}})5p[2\frac{1}{2}]_2$	$(^2P^o_{1\frac{1}{2}})6d[2\frac{1}{2}]^o_3$
20	12	6348 4356.6 ± 0.9	15 751.9120	$2p_9$-$5d'_1$	$(^2P^o_{1\frac{1}{2}})5p[2\frac{1}{2}]_3$	$(^2P^o_{1\frac{1}{2}})6d[2\frac{1}{2}]^o_3$
21	10	6243 1303.0 ± 0.8	16 017.6058	$2p_8$-$4s_5$	$(^2P^o_{1\frac{1}{2}})5p[2\frac{1}{2}]_2$	$(^2P^o_{1\frac{1}{2}})8s[1\frac{1}{2}]^o_2$
22	28	6238 0759.4 ± 1.5	16 030.5839	$2p_9$-$4s_5$	$(^2P^o_{1\frac{1}{2}})5p[2\frac{1}{2}]_3$	$(^2P^o_{1\frac{1}{2}})8s[1\frac{1}{2}]^o_2$
23	19	6224 4540.1 ± 0.6	16 065.6661	$2p_8$-$4s_4$	$(^2P^o_{1\frac{1}{2}})5p[2\frac{1}{2}]_2$	$(^2P^o_{1\frac{1}{2}})8s[1\frac{1}{2}]^o_1$
24	6	6165 3805.0 ± 2.1	16 219.5991	$2p_6$-$6d_5$	$(^2P^o_{1\frac{1}{2}})5p[1\frac{1}{2}]_2$	$(^2P^o_{1\frac{1}{2}})7d[0\frac{1}{2}]^o_1$
25	11	6153 1078.6 ± 1.0	16 251.9498	$2p_6$-$6d_3$	$(^2P^o_{1\frac{1}{2}})5p[1\frac{1}{2}]_2$	$(^2P^o_{1\frac{1}{2}})7d[1\frac{1}{2}]^o_2$
26	23	6084 5440.2 ± 0.9	16 435.0853	$2p_{10}$-$5d_6$	$(^2P^o_{1\frac{1}{2}})5p[0\frac{1}{2}]_1$	$(^2P^o_{1\frac{1}{2}})6d[0\frac{1}{2}]^o_0$
27	11	6076 9360.9 ± 1.1	16 455.6610	$2p_6$-$6d'_1$	$(^2P^o_{1\frac{1}{2}})5p[1\frac{1}{2}]_2$	$(^2P^o_{1\frac{1}{2}})7d[2\frac{1}{2}]^o_3$
28		6057 8021.059	16 507.63729	$2p_{10}$-$5d_5$	$(^2P^o_{1\frac{1}{2}})5p[0\frac{1}{2}]_1$	$(^2P^o_{1\frac{1}{2}})6d[0\frac{1}{2}]^o_1$

29	13	6037 5043.0 ± 0.4	16 563.1352	$2p_7$-$6d''_1$	$(^2P^o_{1\frac{1}{2}})5p[1\frac{1}{2}]_1$	$(^2P^o_{1\frac{1}{2}})7d[2\frac{1}{2}]^o_2$
30	19	6013 8194.3 ± 0.7	16 628.3676	$2p_{10}$-$5d_3$	$(^2P^o_{1\frac{1}{2}})5p[0\frac{1}{2}]_1$	$(^2P^o_{1\frac{1}{2}})6d[1\frac{1}{2}]^o_2$
31	20	5995 5089.5 ± 0.6	16 679.1512	$1s_4$-$2p_4$	$(^2P^o_{1\frac{1}{2}})5s[1\frac{1}{2}]^o_1$	$(^2P^o_{0\frac{1}{2}})5p[1\frac{1}{2}]_1$
32	17	5881 5283.4 ± 3.4	17 002.3834	$1s_4$-$2p_3$	$(^2P^o_{1\frac{1}{2}})5s[1\frac{1}{2}]^o_1$	$(^2P^o_{0\frac{1}{2}})5p[0\frac{1}{2}]_1$
33	16	5872 5418.2 ± 4.3	17 028.4015	$1s_4$-$2p_2$	$(^2P^o_{1\frac{1}{2}})5s[1\frac{1}{2}]^o_1$	$(^2P^o_{0\frac{1}{2}})5p[0\frac{1}{2}]_2$
34	17	5868 3747.0 ± 0.4	17 040.4933	$1s_2$-$3p_{10}$	$(^2P^o_{1\frac{1}{2}})5s[0\frac{1}{2}]^o_1$	$(^2P^o_{1\frac{1}{2}})6p[0\frac{1}{2}]_1$
35	17	5834 4724.0 ± 1.2	17 139.5103	$2p_9$-$6d'_4$	$(^2P^o_{1\frac{1}{2}})5p[2\frac{1}{2}]_3$	$(^2P^o_{1\frac{1}{2}})7d[3\frac{1}{2}]^o_4$
36	10	5828 7049.7 ± 1.6	17 156.4697	$2p_{10}$-$4s_5$	$(^2P^o_{1\frac{1}{2}})5p[0\frac{1}{2}]_1$	$(^2P^o_{1\frac{1}{2}})8s[1\frac{1}{2}]^o_2$
37	14	5826 0988.6 ± 1.5	17 164.1440	$2p_8$-$6d_4$	$(^2P^o_{1\frac{1}{2}})5p[2\frac{1}{2}]_2$	$(^2P^o_{1\frac{1}{2}})7d[3\frac{1}{2}]^o_3$
38	4	5821 6972.2 ± 2.9	17 177.1214	$2p_9$-$6d_4$	$(^2P^o_{1\frac{1}{2}})5p[2\frac{1}{2}]_3$	$(^2P^o_{1\frac{1}{2}})7d[3\frac{1}{2}]^o_3$
39	2	5812 4224.6 ± 0.3	17 204.5306	$2p_{10}$-$4s_4$	$(^2P^o_{1\frac{1}{2}})5p[0\frac{1}{2}]_1$	$(^2P^o_{1\frac{1}{2}})8s[1\frac{1}{2}]^o_1$
40	10	5807 1499.4 ± 0.8	17 220.1512	$2p_8$-$6d''_1$	$(^2P^o_{1\frac{1}{2}})5p[2\frac{1}{2}]_2$	$(^2P^o_{1\frac{1}{2}})7d[2\frac{1}{2}]^o_2$
41	2	5785 4970.3 ± 1.0	17 284.5997	$2p_9$-$6d'_1$	$(^2P^o_{1\frac{1}{2}})5p[2\frac{1}{2}]_3$	$(^2P^o_{1\frac{1}{2}})7d[2\frac{1}{2}]^o_3$
42	2	5752 1549.9 ± 3.2	17 384.7889	$2p_6$-$7d''_1$	$(^2P^o_{1\frac{1}{2}})5p[1\frac{1}{2}]_2$	$(^2P^o_{1\frac{1}{2}})8d[2\frac{1}{2}]^o_2$
43	2	5728 1753.0 ± 3.0	17 457.5663	$2p_9$-$5s_5$	$(^2P^o_{1\frac{1}{2}})5p[2\frac{1}{2}]_3$	$(^2P^o_{1\frac{1}{2}})9s[1\frac{1}{2}]^o_2$

44	2	5725 1512.0 ± 3.0	17 466.7876	$1s_2$-$3p_7$	$(^2P^o_{0\frac{1}{2}})5s[0\frac{1}{2}]^o_1$	$(^2P^o_{1\frac{1}{2}})6p[1\frac{1}{2}]_1$
45	9	5674 0239.8 ± 2.5	17 624.1765	$1s_5$-$2p_4$	$(^2P^o_{1\frac{1}{2}})5s[1\frac{1}{2}]^o_2$	$(^2P^o_{0\frac{1}{2}})5p[1\frac{1}{2}]_1$
46	36	5651 1285.9 ± 2.0	17 695.5803	$1s_3$-$3p_{10}$	$(^2P^o_{0\frac{1}{2}})5s[0\frac{1}{2}]^o_0$	$(^2P^o_{1\frac{1}{2}})6p[0\frac{1}{2}]_1$
47	22	5581 9352.1 ± 0.1	17 914.9338	$1s_2$-$3p_5$	$(^2P^o_{0\frac{1}{2}})5s[0\frac{1}{2}]^o_1$	$(^2P^o_{1\frac{1}{2}})6p[0\frac{1}{2}]_0$
48	22	5571 8352.2 ± 1.9	17 947.4080	$1s_5$-$2p_3$	$(^2P^o_{1\frac{1}{2}})5s[1\frac{1}{2}]^o_2$	$(^2P^o_{0\frac{1}{2}})5p[0\frac{1}{2}]_1$
49	24	5563 7689.5 ± 1.6	17 973.4279	$1s_5$-$2p_2$	$(^2P^o_{1\frac{1}{2}})5s[1\frac{1}{2}]^o_2$	$(^2P^o_{0\frac{1}{2}})5p[1\frac{1}{2}]_2$
50	10	5522 0430.6 ± 1.8	18 109.2394	$2p_9$-$7d'_4$	$(^2P^o_{1\frac{1}{2}})5p[2\frac{1}{2}]_3$	$(^2P^o_{1\frac{1}{2}})8d[3\frac{1}{2}]^o_4$
51	10	5505 8619.0 ± 11.1	18 162.4606	$2p_{10}$-$6d_6$	$(^2P^o_{1\frac{1}{2}})5p[0\frac{1}{2}]_1$	$(^2P^o_{1\frac{1}{2}})7d[0\frac{1}{2}]^o_0$
52	14	5502 2369.0 ± 6.5	18 174.4265	$2p_{10}$-$6d_5$	$(^2P^o_{1\frac{1}{2}})5p[0\frac{1}{2}]_1$	$(^2P^o_{1\frac{1}{2}})7d[0\frac{1}{2}]^o_1$
53	9	5492 4605.1 ± 0.3	18 206.7763	$2p_{10}$-$6d_3$	$(^2P^o_{1\frac{1}{2}})5p[0\frac{1}{2}]_1$	$(^2P^o_{1\frac{1}{2}})7d[1\frac{1}{2}]^o_2$
54	2	5381 1313.3 ± 5.0	18 583.4528	$2p_{10}$-$5s_5$	$(^2P^o_{1\frac{1}{2}})5p[0\frac{1}{2}]_1$	$(^2P^o_{1\frac{1}{2}})9s[1\frac{1}{2}]^o_2$
55	2	5340 6032.6 ± 2.8	18 724.4764	$2p_9$-$8d'_4$	$(^2P^o_{1\frac{1}{2}})5p[2\frac{1}{2}]_3$	$(^2P^o_{1\frac{1}{2}})9d[3\frac{1}{2}]^o_4$
56	4	5229 6319.4 ± 0.1	19 121.8046	$2p_{10}$-$7d_5$	$(^2P^o_{1\frac{1}{2}})5p[0\frac{1}{2}]_1$	$(^2P^o_{1\frac{1}{2}})8d[0\frac{1}{2}]^o_1$
57	5	4813 9798.5 ± 1.5	20 772.8331	$1s_3$-$4X$	$(^2P^o_{0\frac{1}{2}})5s[0\frac{1}{2}]^o_0$	$(^2P^o_{1\frac{1}{2}})4f[1\frac{1}{2}]_1$
58	3	4551 5725.1 ± 2.3	21 970.4288	$1s_4$-$3p_{10}$	$(^2P^o_{1\frac{1}{2}})5s[1\frac{1}{2}]^o_1$	$(^2P^o_{1\frac{1}{2}})6p[0\frac{1}{2}]_1$

59	39	4503	6160.5 ± 0.9	22	204.3795	$1s_4$-$3p_8$	$(^2P^o_{1\frac{1}{2}})5s[1\frac{1}{2}]^o_1$	$(^2P^o_{1\frac{1}{2}})6p[2\frac{1}{2}]_2$
60	21	4464	9416.7 ± 2.1	22	396.7092	$1s_4$-$3p_7$	$(^2P^o_{1\frac{1}{2}})5s[1\frac{1}{2}]^o_1$	$(^2P^o_{1\frac{1}{2}})6p[1\frac{1}{2}]_1$
61	18	4455	1664.9 ± 1.9	22	445.8503	$1s_4$-$3p_6$	$(^2P^o_{1\frac{1}{2}})5s[1\frac{1}{2}]^o_1$	$(^2P^o_{1\frac{1}{2}})6p[1\frac{1}{2}]_2$
62	17	4426	4315.1 ± 0.1	22	591.5616	$1s_2$-$3p_4$	$(^2P^o_{0\frac{1}{2}})5s[0\frac{1}{2}]^o_1$	$(^2P^o_{0\frac{1}{2}})6p[1\frac{1}{2}]_1$
63	12	4420	0007.1 ± 0.5	22	624.4308	$1s_2$-$5z$	$(^2P^o_{0\frac{1}{2}})5s[0\frac{1}{2}]^o_1$	$(^2P^o_{1\frac{1}{2}})5f[1\frac{1}{2}]_2$
64	19	4411	6055.6 ± 0.5	22	667.4844	$1s_2$-$3p_3$	$(^2P^o_{0\frac{1}{2}})5s[0\frac{1}{2}]^o_1$	$(^2P^o_{0\frac{1}{2}})6p[0\frac{1}{2}]_1$
65	24	4401	2010.3 ± 1.8	22	721.0708	$1s_2$-$3p_2$	$(^2P^o_{0\frac{1}{2}})5s[0\frac{1}{2}]^o_1$	$(^2P^o_{0\frac{1}{2}})6p[1\frac{1}{2}]_2$
66	18	4377	3503.2 ± 3.1	22	844.8702	$1s_4$-$3p_5$	$(^2P^o_{1\frac{1}{2}})5s[1\frac{1}{2}]^o_1$	$(^2P^o_{1\frac{1}{2}})6p[0\frac{1}{2}]_0$
67	35	4363	8667.2 ± 1.0	22	915.4570	$1s_5$-$3p_{10}$	$(^2P^o_{1\frac{1}{2}})5s[1\frac{1}{2}]^o_2$	$(^2P^o_{1\frac{1}{2}})6p[0\frac{1}{2}]_1$
68	22	4352	5817.4 ± 1.2	22	974.8701	$1s_2$-$3p_1$	$(^2P^o_{0\frac{1}{2}})5s[0\frac{1}{2}]^o_1$	$(^2P^o_{0\frac{1}{2}})6p[0\frac{1}{2}]_0$
69	17	4301	6953.5 ± 0.4	23	246.6486	$1s_3$-$3p_4$	$(^2P^o_{0\frac{1}{2}})5s[0\frac{1}{2}]^o_0$	$(^2P^o_{0\frac{1}{2}})6p[1\frac{1}{2}]_1$
70	21	4287	6919.7 ± 0.5	23	322.5709	$1s_3$-$3p_3$	$(^2P^o_{0\frac{1}{2}})5s[0\frac{1}{2}]^o_0$	$(^2P^o_{0\frac{1}{2}})6p[0\frac{1}{2}]_1$
71	18	4284	1714.8 ± 0.6	23	341.7361	$1s_5$-$3p_7$	$(^2P^o_{1\frac{1}{2}})5s[1\frac{1}{2}]^o_2$	$(^2P^o_{1\frac{1}{2}})6p[1\frac{1}{2}]_1$
72	21	4275	1714.0 ± 1.1	23	390.8750	$1s_5$-$3p_6$	$(^2P^o_{1\frac{1}{2}})5s[1\frac{1}{2}]^o_2$	$(^2P^o_{1\frac{1}{2}})6p[1\frac{1}{2}]_2$
73	7	4260	5999.9 ± 2.8	23	470.8727	$1s_5$-$3s_1''''$	$(^2P^o_{1\frac{1}{2}})5s[1\frac{1}{2}]^o_2$	$(^2P^o_{0\frac{1}{2}})4d[2\frac{1}{2}]^o_2$

74	2	4185 6492.1 ± 5.1	23 891.1564	$1s_3$-$5p_{10}$	$(^2P^o_{0\frac{1}{2}})5s[0\frac{1}{2}]^o_0$	$(^2P^o_{1\frac{1}{2}})8p[0\frac{1}{2}]_1$
75	16	3992 2074.9 ± 2.1	25 048.7982	$1s_4$-4Z	$(^2P^o_{1\frac{1}{2}})5s[1\frac{1}{2}]^o_1$	$(^2P^o_{1\frac{1}{2}})4f[1\frac{1}{2}]_2$
76	11	3847 0674.9 ± 0.2	25 993.8252	$1s_5$-4Z	$(^2P^o_{1\frac{1}{2}})5s[1\frac{1}{2}]^o_2$	$(^2P^o_{1\frac{1}{2}})4f[1\frac{1}{2}]_2$
77	24	3838 9034.3 ± 0.7	26 049.1054	$1s_5$-4T	$(^2P^o_{1\frac{1}{2}})5s[1\frac{1}{2}]^o_2$	$(^2P^o_{1\frac{1}{2}})4f[2\frac{1}{2}]_3$
78	27	3813 2954.1 ± 0.5	26 224.0370	$1s_4$-$4p_8$	$(^2P^o_{1\frac{1}{2}})5s[1\frac{1}{2}]^o_1$	$(^2P^o_{1\frac{1}{2}})7p[2\frac{1}{2}]_2$
79	37	3801 6206.9 ± 0.5	26 304.5706	$1s_4$-$4p_7$	$(^2P^o_{1\frac{1}{2}})5s[1\frac{1}{2}]^o_1$	$(^2P^o_{1\frac{1}{2}})7p[1\frac{1}{2}]_1$
80	21	3797 9600.3 ± 0.9	26 329.9242	$1s_4$-$4p_6$	$(^2P^o_{1\frac{1}{2}})5s[1\frac{1}{2}]^o_1$	$(^2P^o_{1\frac{1}{2}})7p[1\frac{1}{2}]_2$
81	48	3774 4939.9 ± 0.1	26 493.6175	$1s_4$-$4p_5$	$(^2P^o_{1\frac{1}{2}})5s[1\frac{1}{2}]^o_1$	$(^2P^o_{1\frac{1}{2}})7p[0\frac{1}{2}]_0$
82	5	3699 0956.8 ± 0.6	27 033.6343	$1s_5$-$4p_{10}$	$(^2P^o_{1\frac{1}{2}})5s[1\frac{1}{2}]^o_2$	$(^2P^o_{1\frac{1}{2}})7p[0\frac{1}{2}]_1$
83	39	3680 6069.5 ± 2.3	27 169.4319	$1s_5$-$4p_9$	$(^2P^o_{1\frac{1}{2}})5s[1\frac{1}{2}]^o_2$	$(^2P^o_{1\frac{1}{2}})7p[2\frac{1}{2}]_3$
84	14	3669 7790.9 ± 0.5	27 249.5966	$1s_5$-$4p_7$	$(^2P^o_{1\frac{1}{2}})5s[1\frac{1}{2}]^o_2$	$(^2P^o_{1\frac{1}{2}})7p[1\frac{1}{2}]_1$
85	38	3666 3678.8 ± 0.4	27 274.9498	$1s_5$-$4p_6$	$(^2P^o_{1\frac{1}{2}})5s[1\frac{1}{2}]^o_2$	$(^2P^o_{1\frac{1}{2}})7p[1\frac{1}{2}]_2$
86	2	3633 5219.5 ± 1.8	27 521.5071	$1s_4$-$3p_4$	$(^2P^o_{1\frac{1}{2}})5s[1\frac{1}{2}]^o_1$	$(^2P^o_{0\frac{1}{2}})6p[1\frac{1}{2}]_1$
87	12	3629 1889.5 ± 1.3	27 554.3658	$1s_4$-5Z	$(^2P^o_{1\frac{1}{2}})5s[1\frac{1}{2}]^o_1$	$(^2P^o_{1\frac{1}{2}})5f[1\frac{1}{2}]_2$
88	25	3616 5047.0 ± 0.5	27 651.0079	$1s_4$-$3p_2$	$(^2P^o_{1\frac{1}{2}})5s[1\frac{1}{2}]^o_1$	$(^2P^o_{0\frac{1}{2}})6p[1\frac{1}{2}]_2$

89	2	3541	9632.7 ± 2.1	28 232.9297	$1s_4$-$5p_7$	$(^2P^o_{1\frac{1}{2}})5s[1\frac{1}{2}]^o_1$	$(^2P^o_{1\frac{1}{2}})8p[1\frac{1}{2}]_1$
90	4	3540	5506.9 ± 3.5	28 244.1938	$1s_4$-$5p_6$	$(^2P^o_{1\frac{1}{2}})5s[1\frac{1}{2}]^o_1$	$(^2P^o_{1\frac{1}{2}})8p[1\frac{1}{2}]_2$
91	16	3523	6912.8 ± 1.4	28 379.3307	$1s_4$-$5p_5$	$(^2P^o_{1\frac{1}{2}})5s[1\frac{1}{2}]^o_1$	$(^2P^o_{1\frac{1}{2}})8p[0\frac{1}{2}]_0$
92	19	3503	5538.0 ± 0.5	28 542.4474	$1s_5$-$3p_3$	$(^2P^o_{1\frac{1}{2}})5s[1\frac{1}{2}]^o_2$	$(^2P^o_{0\frac{1}{2}})6p[0\frac{1}{2}]_1$
93	7	3496	9884.0 ± 2.2	28 596.0342	$1s_5$-$3p_2$	$(^2P^o_{1\frac{1}{2}})5s[1\frac{1}{2}]^o_2$	$(^2P^o_{0\frac{1}{2}})6p[1\frac{1}{2}]_2$
94	14	3432	7025.4 ± 1.0	29 131.5658	$1s_5$-$5p_9$	$(^2P^o_{1\frac{1}{2}})5s[1\frac{1}{2}]^o_2$	$(^2P^o_{1\frac{1}{2}})8p[2\frac{1}{2}]_3$
95	12	3425	9224.3 ± 1.9	29 189.2190	$1s_5$-$5p_6$	$(^2P^o_{1\frac{1}{2}})5s[1\frac{1}{2}]^o_2$	$(^2P^o_{1\frac{1}{2}})8p[1\frac{1}{2}]_2$

3.6 Interpretation of the Kr 86 Spectrum and $j\ell$ Coupling

Krypton is the fourth inert gas and in the normal state has the electronic configuration $1s^2 2s^2 2p^6 3s^2 3p^6 3d^{10} 4s^2 4p^6$, $^1S_0$. Thus to emit light, the spherically symmetric atom must have a hole plucked in it. One might expect LS coupling to apply since the core will be an effective charge and the electron will move outside in its field. This is not the case at all for the dominant force is now a magnetic dipole type. No progress can be made using LS coupling ideas, or by relaxing the LS selection rules and going over to jj coupling. Racah (XXV) showed that a third type of coupling, which he named $j\ell$ coupling, could very nicely explain the exceedingly complex spectra of the inert gases, and other heavy atoms with nearly full electron shells.

In the ground state, krypton has no net spin or orbital angular momentum since all of the electrons are paired. However, once the optical electron is extracted to a higher orbit, the core, now designated as $4s^2 4p^5$, has an odd number of electrons and in all cases has a nonzero spin, orbital and total angular momentum. Since the unpaired electron is a p electron and its spin is 1/2, the total angular momentum j of the core will be either $1\frac{1}{2}$ or $0\frac{1}{2}$ depending on whether the spin is parallel or antiparallel to the orbital angular momentum. Thus the core is represented by the symbol $4s^2 4p^5 (^{2s+1}P_j^{\,o})$. Since only one electron is unpaired, $2s + 1 = 2$.

The optical electron is found to interact with the core in two stages. Its orbital angular momentum ℓ adds vectorially with

the total angular momentum, j, of the core to give a new quantum number K.

$$\vec{K} = \vec{j}_{\text{core}} + \vec{\ell}_{\text{optical electron}}$$

The spin of the optical electron now combines vectorially with K to form the total angular momentum of the atom

$$\vec{J} = \vec{K} + \vec{s}_{\text{optical electron}}.$$

The notation started above is now extended as follows

$$4s^2 4p^5 (^2P^o_j) n\ell [K]^o_J$$

The $n\ell$ between the two brackets specifies the optical electron's principal and orbital nomentum quantum numbers. The parity of the entire atom is indicated by a superscript o on the square bracket if odd and ignored if even. Again, the parity designation is superfluous, since the value of ℓ immediately gives the parity. An example will make the notation clear.

Suppose the optical electron is an 8d electron, then $\ell = 2$. If $j = \frac{1}{2}$, $K = 2\frac{1}{2}$ or $1\frac{1}{2}$. Suppose it is $2\frac{1}{2}$. Then $J = 3$ or 2. Suppose it is 3. The term is written as

$$(^2P^o_{0\frac{1}{2}}) 8d[2\tfrac{1}{2}]^o_3$$

As will be observed, the leading terms $4s^2 4p^5$ have been suppressed since they never change. The parity is odd since ℓ of the electron, an even number, is added to ℓ of the core, an odd number.

Since the $j\ell$ notation is not widely appreciated, the older Paschen notation, which is arbitrary, is included in the table of krypton wavelengths for convenience if one wishes to compare this

work with older treatments.

The wavenumbers given in Table VI can be combined in many ways to check on the consistency of the data. An extensive though not complete analysis is presented in Table VII which, for convenience, is broken down into three parts.

Finally, the wavelengths measured here are compared with the recent literature. The agreement is excellent, and argues that the errors as stated in Tables III and IV and VI are very much on the conservative side, as they should be.

Table VII A

Abbreviations used in the analysis of the Kr 86 data.

Abbr.	Paschen	$j\ell$ coupling	
A	$1s_5$-$1s_2$	$(^2P^o_{1\frac{1}{2}})5s[1\frac{1}{2}]^o_1$	$(^2P^o_{1\frac{1}{2}})5s[1\frac{1}{2}]^o_1$
B	$1s_5$-$1s_3$	$(^2P^o_{1\frac{1}{2}})5s[1\frac{1}{2}]^o_1$	$(^2P^o_{1\frac{1}{2}})5s[1\frac{1}{2}]^o_0$
C	$1s_5$-$1s_4$	$(^2P^o_{1\frac{1}{2}})5s[1\frac{1}{2}]^o_2$	$(^2P^o_{1\frac{1}{2}})5s[1\frac{1}{2}]^o_1$
D	$1s_4$-$1s_2$	$(^2P^o_{1\frac{1}{2}})5s[1\frac{1}{2}]^o_1$	$(^2P^o_{0\frac{1}{2}})5s[0\frac{1}{2}]^o_1$
E	$1s_4$-$1s_3$	$(^2P^o_{1\frac{1}{2}})5s[1\frac{1}{2}]^o_1$	$(^2P^o_{0\frac{1}{2}})5s[0\frac{1}{2}]^o_0$
F	$1s_3$-$1s_2$	$(^2P^o_{0\frac{1}{2}})5s[0\frac{1}{2}]^o_0$	$(^2P^o_{0\frac{1}{2}})5s[0\frac{1}{2}]^o_1$
G	$2p_{10}$-$2p_6$	$(^2P^o_{1\frac{1}{2}})5p[0\frac{1}{2}]_1$	$(^2P^o_{1\frac{1}{2}})5p[1\frac{1}{2}]_2$
H	$2p_{10}$-$2p_7$	$(^2P^o_{1\frac{1}{2}})5p[0\frac{1}{2}]_1$	$(^2P^o_{1\frac{1}{2}})5p[1\frac{1}{2}]_1$
I	$2p_{10}$-$2p_8$	$(^2P^o_{1\frac{1}{2}})5p[0\frac{1}{2}]_1$	$(^2P^o_{1\frac{1}{2}})5p[2\frac{1}{2}]_2$
J	$2p_{10}$-$2p_9$	$(^2P^o_{1\frac{1}{2}})5p[0\frac{1}{2}]_1$	$(^2P^o_{1\frac{1}{2}})5p[2\frac{1}{2}]_3$
K	$2p_9$-$2p_6$	$(^2P^o_{1\frac{1}{2}})5p[2\frac{1}{2}]_3$	$(^2P^o_{1\frac{1}{2}})5p[1\frac{1}{2}]_2$
L	$2p_9$-$2p_7$	$(^2P^o_{1\frac{1}{2}})5p[2\frac{1}{2}]_3$	$(^2P^o_{1\frac{1}{2}})5p[1\frac{1}{2}]_1$
M	$2p_9$-$2p_8$	$(^2P^o_{1\frac{1}{2}})5p[2\frac{1}{2}]_3$	$(^2P^o_{1\frac{1}{2}})5p[1\frac{1}{2}]_2$
N	$2p_8$-$2p_6$	$(^2P^o_{1\frac{1}{2}})5p[2\frac{1}{2}]_2$	$(^2P^o_{1\frac{1}{2}})5p[1\frac{1}{2}]_2$
O	$2p_8$-$2p_7$	$(^2P^o_{1\frac{1}{2}})5p[2\frac{1}{2}]_2$	$(^2P^o_{1\frac{1}{2}})5p[1\frac{1}{2}]_1$
P	$2p_7$-$2p_6$	$(^2P^o_{1\frac{1}{2}})5p[1\frac{1}{2}]_1$	$(^2P^o_{1\frac{1}{2}})5p[1\frac{1}{2}]_2$

Table VII B

Consistency of the Kr 86 Wavelengths

Transition	Lines	Wavenumber Difference
A	71-44	5 874.9485
A	92-64	5 874.9630
A	93-65	5 874.9635
Average		5 874.9583
B	67-46	5 219.8765
B	92-70	5 219.8766
Average		5 219.8765
C	45-31	945.0253
C	48-32	945.0246
C	49-33	945.0264
C	67-58	945.0281
C	71-60	945.0269
C	72-61	945.0278
C	76-75	945.0270
C	84-79	945.0260
C	93-88	945.0263
C	95-90	945.0251
Average		945.0260
D	58-31	4 929.9355
D	60-44	4 929.9216
D	66-47	4 929.9364
D	86-62	4 929.9455

D	87-63	4 929.9451
D	88-65	4 929.9371
Average		4 929.9369
E	58-46	4 274.8485
E	86-69	4 274.8585
Average		4 274.8535
F	69-62	655.0870
F	70-64	655.0866
F	46-34	655.0870
Average		655.0868
G	28-2	1 954.8264
G	30-5	1 954.8270
G	36-9	1 954.8254
G	39-10	1 954.8276
G	52-24	1 954.8274
Average		1 954.8267
H	26-4	1 795.8795
H	30-6	1 795.8800
H	39-13	1 795.8800
Average		1 795.8798
I	28-12	1 138.8642
I	36-21	1 138.8639
I	39-23	1 138.8644
Average		1 138.8642

J	54-43	1 125.8865
J	30-15	1 125.8864
J	36-22	1 125.8857
Average		1 125.8862
K	15-5	828.9406
K	20-7	828.9400
K	22-9	828.9396
K	41-27	828.9387
Average		828.9398
L	15-6	669.9936
M	17-16	12.9770
M	20-9	12.9767
M	22-21	12.9781
M	38-37	12.9774
Average		12.9773
N	12-2	815.9622
N	19-7	815.9633
N	21-9	815.9615
N	23-10	815.9631
Average		815.9625
O	18-8	657.0153
O	23-13	657.0155
O	40-29	657.0160
Average		657.0156
P	6-5	158.9470

The average values of the transitions may be combined in numerous ways to yield level differences. Some of the possibilities are included in Table VII C.

Table VII C

Combinations of the average transitions

A	5 874.9583
B + F	5 874.9633
C + D	5 874.9711
C + E + F	5 874.9663
B	5 219.8765
C + E	5 219.8795
A - F	5 219.8715
C	945.0260
A - D	945.0214
B - E	945.0230
D	4 929.9369
A - C	4 929.9323
E	4 274.8535
B - C	4 274.8505
D - F	4 274.8501
F	655.0868
A - B	655.0818
D - E	655.0834

G	1 954.8267
J + M + O + P	1 954.8261
I + N	1 954.8267
H + P	1 954.8268
J + K	1 954.8260
H	1 795.8798
G - P	1 795.8797
I + O	1 795.8798
J + L	1 795.8798
I	1 138.8642
G - N	1 138.8642
H - O	1 138.8642
J + M	1 138.8635
J	1 125.8862
I - M	1 125.8869
H - L	1 125.8862
G - K	1 125.8869
K	828.9398
M + O + P	828.9399
G - J	828.9404
M + N	828.9398
P + H - J	828.9406
L	669.9936
M + O	669.9929

H - J	669.9936
K - P	669.9928
M	12.9773
I - J	12.9780
L - O	12.9780
K - N	12.9773
N	815.9625
O + P	815.9625
K - M	815.9625
G - I	815.9625
O	657.0156
N - P	657.0155
H - I	657.0156
L - M	657.0163
P	158.9470
G - H	158.9469
K - L	158.9462
N - O	158.9469

Virtually every difference listed above is accurate to 5 millikaysers or better. In particular, differences G, H, J, K and P are consistent to about 0.5 millikaysers while difference N shows no variation in the fourth decimal place. Quite likely, the poorer values can be attributed to the small number of interference patterns measured for some of the lines. For example,

line 44 gives low values of A and D, which is not surprising at all for it was measurable only twice on one plate.

3.7 Comparison of the Author's Data with the Recent Literature

Table VIII

All entries in 10^{-14} m.

Phelps	Baird et al (XI)	International Committee(X)
	Krypton 86	
6458 0718.4	6458 0718.8	6458 0720
6422 8005.7	6422 8004.8	6422 8006
6013 8194.3	6013 8196.0	
5651 1285.9	5651 1285.8	5651 1286
5563 7689.5	5563 7691.4	
4503 6160.5	4503 6162.2	4503 6162
4464 9416.7	4464 9417.2	
4377 3503.2	4377 3502.5	
	Mercury 198	
5792 2689.5*	5792 2683.8*	5792 2683*
5771 1994.0	5771 1982.7	5771 1983
5462 2711.3	5462 2705.1	5462 2705
4359 5625.2	4359 5622.7	4359 5624
4047 7147.9	4047 7145.3	

*Double line, unresolved.

Bibliography

I. Hart, K. H. and Baird, K. M. On the Relation Between the Old and the New Definition of the International Meter. Canadian Journal of Physics 39, 6, 781-789 June 1961.

II. Jenkins, F. A. and White, H. E. Fundamentals of Optics 2nd Edition, 1950. McGraw Hill Book Company, New York.

III. Meissner, K. W. Interference Spectroscopy. Journal of the Optical Society of America. Part I. 31, 405-427 June 1941. Part II. 32, 182-211 April 1942.

IV. Baird, K. M. and Smith, D. S. Primary Standard of Length. Journal of the Optical Society of America 52, 5, 507-514 May 1962.

V. Strong, J. et al. Procedures in Experimental Physics. Prentice Hall, Inc., New York 1938.

VI. Smith, A. W. Precision Determination of Argon Wavelengths in the Region 3900 Å to 4600 Å. Unpublished Master's Thesis, Library, University of Alberta, 1952.

VII. Olafson, R. A. Ultraviolet Dispersion of Air. Unpublished Master's Thesis, Library, University of Alberta, 1956.

VIII. Komhyr, W. D. Dispersion of Air in the Region 2000 Å to 7000 Å. Unpublished Master's Thesis, Library, University of Alberta, 1956.

IX. Schultz, A. A. Precision Measurements of the Mercury 198 Wavelengths. Unpublished Master's Thesis, Library, University of Alberta, 1956.

X. International Committee on Weights and Measures. Technical Note. Journal of the Optical Society of America 53, 3, 401, March 1963.

XI. Baird, K. M., Smith, D. S., and Hart, K. H. Vacuum Wavelengths of Kr 86, Hg 198, and Cd 114. Journal of the Optical Society of America 53, 6, 717-720, June 1963.

XII. Harrison, G. R. Massachusetts Institute of Technology Wavelength Tables. John Wiley and Sons, Inc., New York 1939.

XIII. Moore, C. E. Atomic Energy Levels Vol. II, Circular 467, National Bureau of Standards 1952. U. S. Government Printing Office, Washington, D. C.

XIV. Grotrian, W. Graphische Darstellung der Spektren von Atomen und Ionen mit Ein, Zwei und Drei Valenzelektronen Springer Verlag, Berlin, 1928.

XV. Sawyer, R. A. Experimental Spectroscopy, 2nd Edition 1951. Prentice Hall, Englewood Cliffs, New Jersey.

XVI. Harrison, G. R., Lord, R. C., and Loofbourow, J. R. Practical Spectroscopy. Prentice Hall, Englewood Cliffs, New Jersey, 1948.

XVII. Parratt, Lyman G. Probability and Experimental Errors in Science. John Wiley and Sons, New York, 1961.

XVIII. Jackson, C. V. Wavelength Standards in the First Spectrum of Krypton. Royal Society Philosophical Transactions 236 A, pp 1-24, August 24, 1936.

XIX. Jackson, C. V. Interferometric Measurements in the Spectrum of Krypton. Proceedings of the Royal Society, Series A, Vol. 138, pp 147-153, 1932.

XX. Baird, K. M., and Smith, D. S. Kr 86 and Hg 198 Wavelength Standards. Canadian Journal of Physics 37, 7 pp 832-840, July 1959.

XXI. Condon, E. U. and Odishaw, H. (Editors). Handbook of Physics. McGraw-Hill Book Company, New York, 1958.

XXII. White, H. E. Introduction to Atomic Spectra. McGraw Hill Book Company, New York, 1934.

XXIII. Semat, H. Introduction to Atomic and Nuclear Physics 3rd Edition, 1954, Reinhard and Company, New York.

XXIV. Landolt-Börnstein (Editors) Zahlenwerte und Funktionen aus Physik, Chemie, Astronomie, Geophysik, Technik. Springer Verlag, Berlin, 1950.

XXV. Racah, G. On a New Type of Vector Coupling in Complex Spectra. Physical Review 61, 537, April 1942.

XXVI. Kuhn, H. G. Atomic Spectra. Longmans, Green and Company Limited, London, 1961.

XXVII. Tolansky, S. High Resolution Spectroscopy. Methuen and Company, London, 1947.

XXVIII. Kaufman, V. Wavelengths and Pressure Shifts in Mercury 198. Journal of the Optical Society of America 52, 8, p 866, August 1962.

Appendix I

Aluminization of the Etalon Mirrors

The method followed in aluminizing the Fabry-Perot etalon mirrors parallels that found in Strong (V) p. 171 et seq. except for certain modifications discussed below.

An all glass still was constructed without demountable joints so that distilled water from the building supply could be redistilled and kept free of contamination. The redistilled water is stored in a flask with an inverted beaker as a cover. A holder for the two mirrors and a movable filament shield were constructed and installed in the vacuum chamber. A photocell was mounted above, and a 6 watt light below the mirrors in such positions that no aluminum was deposited on either during the evaporation acts as a variable reflectivity mirror and reflects additional light into the photocell. An empirical calibration curve was obtained from a trial run. A helical filament was wound from 1. mm tungsten wire in each loop of which is crimped a small piece of pure aluminum.

The entire aluminum coating should be deposited in a few seconds but some practice is required to obtain 90.% reflectivity. The usual result is a coating of 99.% reflectivity. In the remaining steps of the procedure, it is advisable to wear surgical gloves to prevent the hands from dissolving and to prevent oil from the skin from contaminating the optical flats.

1. The entire vacuum chamber, bell jar, electrode shields, and all demountable parts are scrubbed with a 10.% KOH solution

followed by a thorough rinsing in tap water and then in distilled water. All exposed surfaces are dried with lint-free paper towels such as Kimwipes.

2. The mirrors are placed on lens paper in petri dishes and covered with a 5% KOH solution. The surfaces are scrubbed with lens paper until all traces of old aluminum are removed. They are washed with tap water and given a final rinsing with distilled water.

3. The damp mirrors are placed on sheets of Kimwipes to protect them from scratches. Reagent grade $CaCO_3$, precipitated chalk, is rubbed vigorously into the surface with a piece of lens paper. Additional chalk and distilled water are added as necessary until each surface has been scrubbed for 5 minutes. The mirrors are washed thoroughly in distilled water and rinsed with redistilled water.

If, at this point, the redistilled water wets the entire surface and does not pull back leaving a dry area, the remaining steps in the procedure may be carried out. If this test fails, additional rubbing with chalk will be necessary until the test is positive. If the test is ignored, poor adhesion between the quartz flat and the film will result.

4. The mirrors are dried carefully with lens paper. Any bits of lint left behind can be blown off with a gentle puff of air or removed with a sable hair brush which has been soaked in acetone to remove all traces of oil from the hairs and then washed in a strong detergent and dried.

5. The mirrors are placed on the rack. The bell jar is

sealed and evacuated under a glow discharge. Two hours after the glow stops, the pressure should be about 10^{-4} torr. At this pressure the filament is outgassed and the aluminum fused with a current of 15 amperes for three minutes or until a coating of aluminum forms on the bell jar wall below the filament shield. The pressure will drop very rapidly when the filament current ceases due to the gettering action of the aluminum film. At a pressure of 10^{-5} torr or less, the shield is moved aside exposing the mirrors to the filament. The aluminum coating is evaporated rapidly with a current of 18 amperes for 10 seconds. The empirical calibration curve of the photocell will help the operator shut off the filament current when a film of the correct thickness has been formed. The vacuum is then broken and the bell jar removed so that an accurate measurement of the transmissivity can be made. If too much or too little aluminum has been deposited, the entire procedure must be started again with the cleaning of the bell jar, etc.

Appendix II

The Intensity Distribution of Fabry-Perot Interference Fringes

Since the two reflecting surfaces of a Fabry-Perot etalon are assumed to be identical, each surface has a reflection coefficient ρ and a transmission coefficient σ. Consider an incident electromagnetic wave $e^{i\omega t}$ of amplitude 1. The first partial wave, which passes straight through the etalon, will have amplitude $\sigma^2 e^{i\omega t}$. The second partial wave, which makes two reflections inside the etalon and therefore has a phase difference of $2\pi p$ from the first partial wave, will have amplitude $\sigma^2\rho^2 e^{i(\omega t-2\pi p)}$. The n^{th} partial wave will have amplitude $sr^n e^{i(\omega t-2\pi np)}$. We have set $\sigma^2=s$ and $\rho^2=r$, the transmission and reflection "powers" respectively.

The sum of all the partial waves, practically an infinite number, will give the resultant amplitude of the transmitted wave at infinity, or in fact, in the focal plane of the lens used to project the fringes on the slit of the spectrograph. Thus

$$Ae^{i\omega t} = se^{i\omega t} \sum_{n=1}^{\infty} r^n e^{-i2\pi np}$$

The terms of the sum form a geometric progression with common ratio $re^{-i2\pi p}$ whose sum is

$$A = \frac{se^{i\omega t}}{1 - re^{-i\omega t}}$$

The observable intensity $I = AA^*$. Hence,

$$I = \frac{se^{i\omega t}se^{-i\omega t}}{(1 - re^{i2\pi p})(1 - re^{-i2\pi p})}$$

$$= \frac{\dfrac{s^2}{(1-r)^2}}{1 + \dfrac{4r}{(1-r)^2}\sin^2\pi p} \qquad (1)$$

For p an integer we find $I_{max} = s^2/(1-r)^2$; and for p an integer plus $\frac{1}{2}$ we find $I_{min} = s^2/(1+r)^2$. Thus, as we progress outward along a radius of the ring system, the intensity should alternate between these two values. Suppose, however, that p in an integer and that γ is a small fractional part of the adjacent order number. Then near the maximum, at order number $(p\pm\gamma)$, (1) becomes

$$I = \frac{I_{max}}{1 + \dfrac{4r}{(1-r)^2}\sin^2\pi\gamma}$$

$$\doteq \frac{I_{max}}{1 + \eta^2\pi^2\gamma^2} \qquad (2)$$

where $\eta^2 = 4r/(1-r)^2$. Expanding in a binomial series gives,

$$I = I_{max}(1 - \eta^2\pi^2\gamma^2 + \ldots.)$$

which, to first order, is parabolic in the order number γ.